JOURNAL OF GEOPHYSICAL RESEARCH, VOL. 102, NO. D22, PAGES 26,033–26,052, NOVEMBER 27, 1997

Mean winds in the tropical stratosphere and mesosphere during January 1993, March 1994, and August 1994

Matthew II. Hitchman,[1] Erhan Kudeki,[2] David C. Fritts,[3] Joleen M. Kugi,[1] Clint Fawcett,[2] Gregory A. Postel,[1] Chia-Yi Yao,[1] David Ortland,[4] Dennis Riggin,[3] and V. Lynn Harvey[1]

Abstract. Radar observations of winds and momentum fluxes in the stratosphere and mesosphere at the Jicamarca Radio Observatory in Peru (JRO; 12°S, 77°W) were taken during three 10 day campaigns in January 1993, March 1994, and August 1994. In order to interpret features in the campaign mean JRO wind profiles, we examined global circulation patterns as depicted by long time series of radiosonde profiles, analyses from the European Center for Medium Range Weather Forecasting (ECMWF), and winds from the High Resolution Doppler Imager (HRDI) aboard the Upper Atmosphere Research Satellite. In the tropical stratosphere, large-scale analyses show that a geographically varying annual cycle significantly affects winds over JRO, as does the quasi-biennial oscillation (QBO). The spatial structure of the annual cycle and QBO is shown for the three campaigns, emphasizing the upward influence of subtropical tropospheric monsoon anticyclones. These anticyclones tilt poleward and merge zonally, underlying the zonal summer easterlies, which also merge zonally and tilt poleward with altitude. The annual cycle at Singapore includes a substantial easterly acceleration during March-August, which causes an apparent stalling of descending QBO westerlies or a more rapid descent of QBO easterlies. In the mesosphere, JRO and HRDI winds agree reasonably well, with zonal winds over JRO varying on a semiannual basis and meridional winds exhibiting structures expected from the diurnal tide. For vertical motion, separate north-south and east-west beam pair estimates agree, yet campaign-averaged vertical motions are large: ~1-5 cm/s in the stratosphere and ~10-50 cm/s in the mesosphere. In both the stratosphere and mesosphere, vertical winds are anticorrelated with horizontal wind. Possible explanations for the large vertical motions include aspect sensitivity and the diurnal tide. Uncertainties in the meaning of radar vertical motions create a challenge for interpreting momentum fluxes.

1. Introduction

Mesosphere-stratosphere-troposphere (MST) radars have proven to be extremely useful in depicting local variability with high temporal and spatial resolution. They are a primary means of estimating the contribution of subsynoptic-scale motions to the general circulation of the middle atmosphere. They are also a primary means of estimating vertical motions and momentum fluxes. Large-scale phenomena such as the annual cycle and the quasi-biennial oscillation (QBO) also affect radar wind profiles. In this paper we describe results from three 10 day campaigns at the Jicamarca Radar Observatory (hereafter JRO), at 12°S, 77°W near Lima, Peru, during three different seasons. Global data sets are used to interpret the JRO profiles. The JRO data provide simultaneous information from the lower stratosphere and mesosphere, reflecting processes over a wide range of scales. In order to understand the data it is necessary to consider rather disparate phenomena, ranging in altitude from subtropical monsoon structures in the lowest stratosphere to the diurnal tide in the mesosphere and in scale from the zonally symmetric QBO down to gravity wave motions.

A prevailing view of the tropical stratospheric general circulation is that the flow is dominated by the zonal mean QBO and the tropical planetary waves which drive it. Here we explore the contribution of

[1] Department of Atmospheric and Oceanic Sciences, University of Wisconsin-Madison.
[2] Department of Electrical and Computer Engineering, University of Illinois, Urbana.
[3] Colorado Research Associates, Boulder.
[4] Space Physics Research Laboratory, Department of Atmospheric, Oceanic and Space Sciences, University of Michigan, Ann Arbor.

Paper number 97JD01784.
0148-0227/97/97JD-01784$09.00

monsoon structures and gravity waves to the stratospheric general circulation. It may be of historical interest to note *Dove's* [1837] view of the extratropical troposphere as being most fundamentally the synoptic-scale zonal asymmetries themselves, where the transient eddies accomplish virtually all of the transport of momentum, heat, and constituents. Similarly, *Bjerknes et al.* [1933] viewed the tropical tropospheric circulation as being most fundamentally the zonally asymmetric monsoon circulations, which account for virtually all of the heat and momentum transports. In attempting to reconcile differences between stratospheric winds over Jicamarca during 1987 and "correlative" tropical winds at sites far removed geographically, *Hitchman et al.* [1992] suggested that the differences are due to the upward extension of tropical monsoon structures into the stratosphere. One goal of the present work is to contribute toward a better understanding of the tropical "stratospheric geography" (coined by A. Tuck). We use this phrase to suggest a physical relationship between regional stratospheric features and properties of the underlying continents and oceans. It is essential to take into account these continental-scale variations if one hopes to understand the distribution of winds and hence of local gravity wave driving throughout the tropics.

The earliest mention of the significance of small-scale processes is probably *Helmholtz'* [1888] realization that the upper branch of the *Hadley* [1735] circulation requires in situ friction to explain the marked depression of observed zonal flow speeds relative to angular momentum conserving flow. He envisaged differential horizontal motions in the vertical leading to an unstable surface of discontinuity, giving rise to small- and medium-scale vortices. These would then mix angular momentum, thereby reducing wind speeds aloft. This type of mechanism is a primary means by which inertio-gravity waves can be absorbed and influence the larger-scale circulation [e.g., *O'Sullivan and Dunkerton,* 1995]. Helmholtz' work anticipated what is now called the body force due to gravity wave momentum flux convergence, or "gravity wave driving." It has been known since ~1960 that gravity wave driving is essential to the mesospheric general circulation [*Haurwitz,* 1961; *Leovy,* 1964]. More recently, it has become increasingly clear that gravity waves also exert an important influence on the tropical and subtropical stratosphere [e.g., *Teweles,* 1958; *Kitaoka,* 1962; *Palmer et al.*, 1986; *Tanaka and Yamanaka*, 1985; *Hitchman and Leovy,* 1988; *Iwasaki et al.*, 1989; *Hitchman et al.,* 1992; *Bergman and Salby,* 1994; *Ogino et al.*, 1995; S. J. Allen and R. A. Vincent, Gravity wave activity in the lower atmosphere: Seasonal and latitudinal variations, submitted to *Journal of Geophysical Research*, 1996]. Owing to the challenge of quantifying the effects of small-scale motions for all locations and times, the angular momentum budget in the tropical middle atmosphere remains largely unsolved.

Although MST radars offer a unique opportunity to quantify momentum fluxes by small-scale motions, it will be shown that campaign mean vertical motions often contribute substantially to momentum fluxes. Theoretical studies of large-scale tropical phenomena suggest very weak vertical motions for a self-consistent circulation. Yet even weak vertical advection can markedly influence the descent rates of QBO shear zones, as originally suggested by *Lindzen and Holton* [1968]. Since estimated vertical motion magnitudes typically exceed 10 cm/s at JRO, as well as at other MST radar sites [e.g., *Coy et al.* 1986; *Cornish* 1988; *Hoppe and Fritts*, 1995], it is important to understand what they mean. This problem is compounded by the fact that nonzero time mean vertical and horizontal motions imply a nonzero momentum flux, requiring a careful interpretation of body force estimates. We seek to promote discussion of these issues in the broader scientific community.

Mesospheric observations are possible at Jicamarca only during the daytime, due to the availability of free electrons required for radar backscattering from turbulent inhomogeneities. Hence a campaign average of daytime mesospheric observations is a useful way to depict the diurnal tide. One benefit of using data at 12°S is that, while the meridional wind should be affected by the diurnal tide, the zonal wind component is expected to have only a small diurnal tide contribution. Zonal wind variations are expected from the mesopause semiannual oscillation (MSAO). Directly sensed mesospheric winds from the High Resolution Doppler Imager (HRDI) exhibit similar tidal and MSAO variations, supporting the features seen in mesospheric JRO winds.

These JRO measurements were part of a more extensive set of observations throughout the tropics during 1993-1994 known as the CADRE (Coupling and Dynamics of Regions Equatorial) campaigns. Section 2 provides a description of the JRO configuration for CADRE, data analysis methods, and the data sets used for comparison. Campaign mean profiles of horizontal winds and data frequency are introduced in section 3 for both the stratosphere and mesosphere. Stratospheric horizontal winds are interpreted in terms of geographical variation in the annual cycle and the phase of the quasibiennial oscillation. Mesospheric horizontal winds are interpreted in terms of the diurnal tide and MSAO. The difficult issues of interpreting vertical motions and the implications for momentum fluxes are dealt with in section 4. Conclusions are given in section 5.

2. Data and Analysis

2.1. Jicamarca Radar

Wind and momentum flux measurements were taken at JRO (12°S, 77°W) during January 20-29, 1993, March 10-19, 1994, and August 16-25, 1994. The radar was configured to have four independent beams steered 2.5° from the zenith in the geomagnetic north, south, east, and west directions. Each of the four beams has ~0.6° radial and ~1.5° azimuthal half widths. The separation between beam pairs is ~2 km at 20 km altitude and ~7 km at 80 km altitude, with the half-power width at 80 km being ~1 km. The JRO radar emits at 50

MHz (6 m wavelength). Using the technique of *Spano et al.* [1991], discrete power spectra were estimated from the backscattered signal in the range 10-130 km at 400 m resolution. Line-of-sight mean Doppler velocity estimates were combined to estimate meteorological wind components and momentum fluxes.

Useful signal returns result from vertical variations of refractive index below ~32 km at all times and from electron density fluctuations in the mesosphere during daylight hours only. About 10 hours of data were taken each day during daytime, which contain tidal information that cannot be removed by averaging. To avoid possible contamination of Doppler winds by plasma waves, mesospheric profiles which begin at 60 km are truncated near 85 km, coincident with the minimum in echo frequency for each campaign. Stratospheric profiles begin at 19.2 km for January 1993 and March 1994 but at 9.2 km for the August 1994 campaign. In the stratosphere, 256 point fast Fourier transforms (FFTs) and line-of-sight velocity limits of ~2.5 m/s allowed for a possible horizontal wind range of ~ ±55 m/s and resolution of ~0.45 m/s. In the mesosphere, 64 point FFTs (128 point FFTs for August) and line-of-sight velocity limits of 3.5-7.0 m/s allowed for a horizontal wind range of ~ ±80-160 m/s and resolution of ~1.2-5.0 m/s. Vertical motion resolution was ~1-2 mm/s. Coherent averaging was applied to give 2 min estimates in the stratosphere and 1 min estimates in the mesosphere. A detectability parameter was defined which is proportional to the ratio of the maximum value of the power spectrum (at the wind-induced Doppler-shifted frequency) to the noise density (the average of the rest of the power spectrum). A wind estimate was excluded in averaging if the associated detectability fell below 3.0. In addition, a campaign average value was not plotted if the associated data count value fell below 10% of the maximum of the count profile. Further information about the experimental design is given by *Riggin et al.* [this issue], *Fritts et al.* [1992], and *Hitchman et al.* [1992].

Estimates of zonal and meridional velocity components are obtained from line-of-sight velocities using

$$u_{\mathrm{ew}}(z) = \frac{U_{\mathrm{e}}(R) - U_{\mathrm{w}}(R)}{2 \sin \theta} \tag{1a}$$

$$v_{\mathrm{ns}}(z) = \frac{U_{\mathrm{n}}(R) - U_{\mathrm{s}}(R)}{2 \sin \theta} \tag{1b}$$

while separate estimates of vertical motion are obtained from the east-west and north-south beam pairs:

$$w_{\mathrm{ew}}(z) = \frac{U_{\mathrm{e}}(R) + U_{\mathrm{w}}(R)}{2 \cos \theta} \tag{2a}$$

$$w_{\mathrm{ns}}(z) = \frac{U_{\mathrm{n}}(R) + U_{\mathrm{s}}(R)}{2 \cos \theta}, \tag{2b}$$

where the subscripts e, w, n, s correspond to radar beams directed toward magnetic east, west, north, and south, θ is the zenith angle, and $R = c\,T/2$ is the target range, where c is the speed of light, T is the sampling delay, and $z = R \cos \theta$ is the geometric height [*Vincent and Reid*, 1983]. Since geomagnetic north is 6°01′ east of geographic north, horizontal velocity estimates u_{ew} and v_{ns} were rotated to obtain meteorological wind components u and v. These were used, together with vertical motion estimates w_{ew} and w_{ns}, to estimate momentum fluxes in the two planes.

Considerable variability is evident in the data at timescales down to the buoyancy frequency. In both the stratosphere and mesosphere, echo returns are episodic, characterized by thin layered turbulence [*Woodman and Guillen*, 1974]. To obtain more continuous vertical coverage and more stable statistical estimators, we focus on the campaign average profiles $\overline{u}$, $\overline{v}$, $\overline{w}_{\mathrm{ew}}$, and $\overline{w}_{\mathrm{ns}}$, where overbars indicate the campaign time average. The zonal and meridional momentum fluxes per unit mass, or covariances between horizontal and vertical winds, were calculated by the direct estimators $\overline{u(t)\,w(t)}$ and $\overline{v(t)\,w(t)}$ and separately by the method of *Vincent and Reid* [1983]. We found precise agreement for the campaign averages, verifying empirically the algebraic equivalences

$$\overline{uw}(z) = \frac{\overline{U_{\mathrm{e}}^2}(R) - \overline{U_{\mathrm{w}}^2}(R)}{2 \sin 2\theta} \tag{3a}$$

$$\overline{vw}(z) = \frac{\overline{U_{\mathrm{n}}^2}(R) - \overline{U_{\mathrm{s}}^2}(R)}{2 \sin 2\theta} \tag{3b}$$

under the assumption of statistical homogeneity across the radar beams.

As in the 1987 campaigns [*Hitchman et al.*, 1992], it was found that $\overline{w}(z)$ is often substantial, implying that the time mean circulation contributes significantly to the Reynolds stresses. We therefore separately calculated $\overline{u}\,\overline{w}$ and $\overline{v}\,\overline{w}$ and the stresses associated with motions having timescales of less than 10 days: $\overline{u'w'} = \overline{uw} - \overline{u}\,\overline{w}$ and $\overline{v'w'} = \overline{vw} - \overline{v}\,\overline{w}$.

2.2. Comparison Data Sets

Long time series (~35 years) of radiosonde data at 15 widely spaced tropical stations at standard pressure levels were obtained from the National Center for Atmospheric Research (NCAR) and used to create monthly mean annual composites for depicting the annual cycle in the tropical stratosphere [*Yao*, 1994]. These are consistent with geographical variations of the annual cycle in the stratosphere seen in 8 years of monthly averaged ECMWF analyses [*Postel*, 1994]. Other recent work regarding transport across the subtropical lower stratosphere by quasi-stationary zonal asymmetries includes *Trepte et al.* [1993], *Hitchman et al.* [1994], *Chen* [1995], and *Dunkerton* [1995].

ECMWF analyses include satellite data and are described by *Hollingsworth et al.* [1986] and *Trenberth and Olson* [1988]. Care must be taken in interpreting tropical stratospheric analyses. Here only the most robust, coherent features are examined for agreement between ECMWF and JRO winds. Values in Figures 7, 8, and 10 are campaign averages of twice daily ECMWF data at 2 1/2° resolution. HRDI observations employ

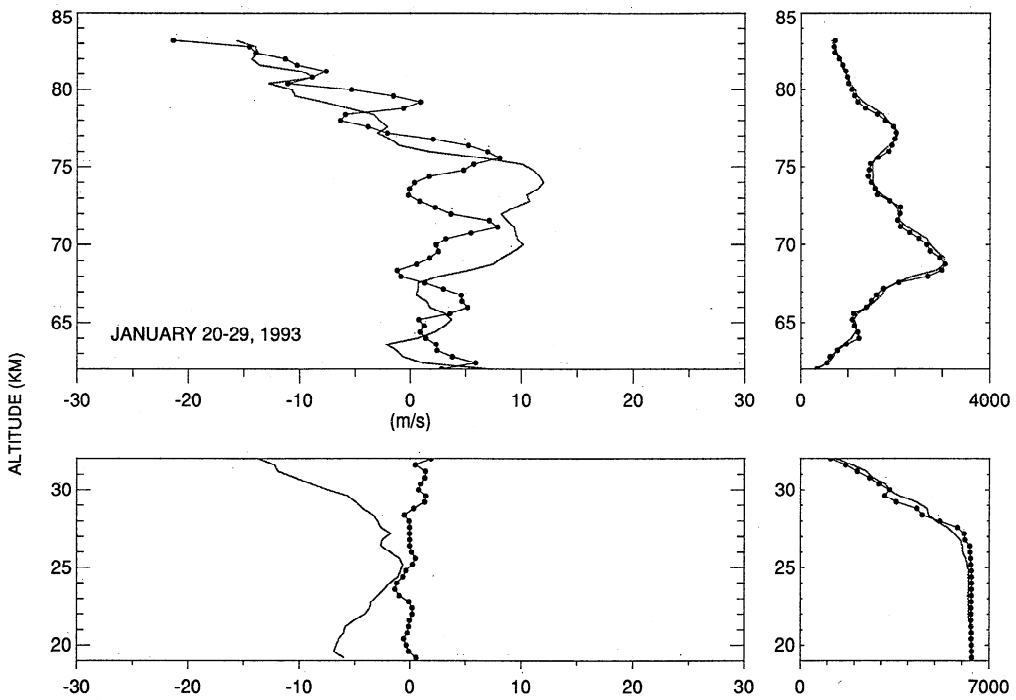

Figure 1. Campaign average horizontal wind and data count profiles at Jicamarca Radio Observatory (12°S, 77°W) for zonal (thin line, east-west beam pair), and meridional (thin line with dots, north-south beam pair) components during January 20-29, 1993. The speed range is ±30 m/s. Note that the data count range differs in the two layers.

Doppler-shifted molecular oxygen visible emission lines to infer bulk air motions in the mesosphere [*Hays et al.*, 1993, 1994], while O_2 absorption lines are used to infer stratospheric winds (not shown) [*Ortland et al.*, 1996]. METEOSAT visible and infrared images of the South American sector were also archived for each of the campaign days, as an indicator of the degree of convection.

3. Horizontal Winds

3.1. JRO Wind and Data Count Profiles

Figures 1, 2, and 3 show campaign mean profiles of zonal (thin line) and meridional (thin line connecting dots at observation levels) wind components and data

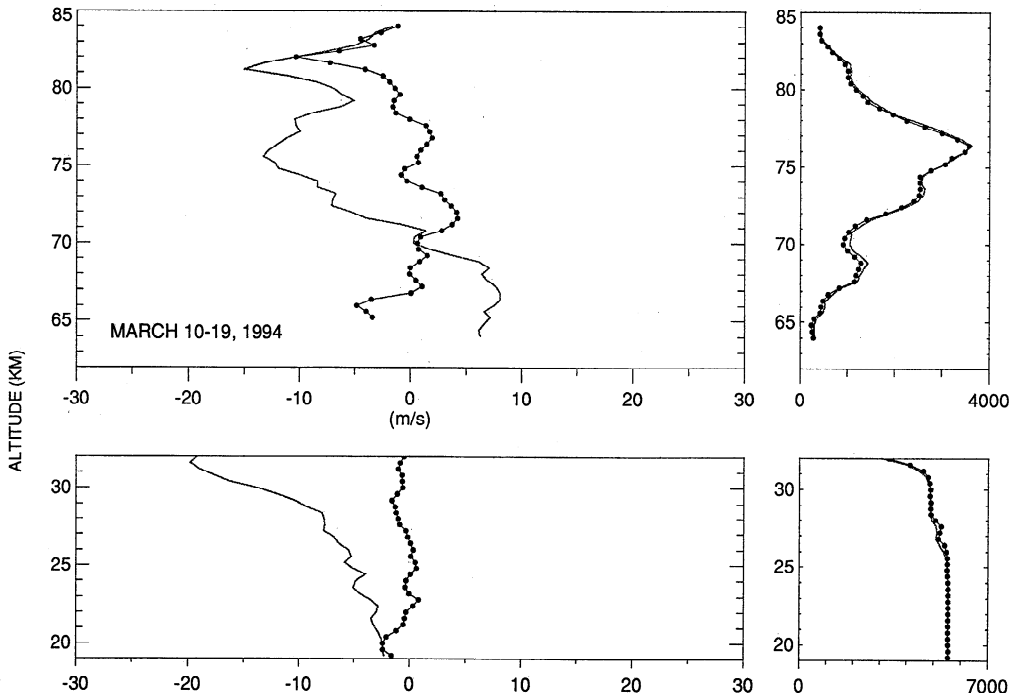

Figure 2. As in Figure 1 except for the period March 10-19, 1994.

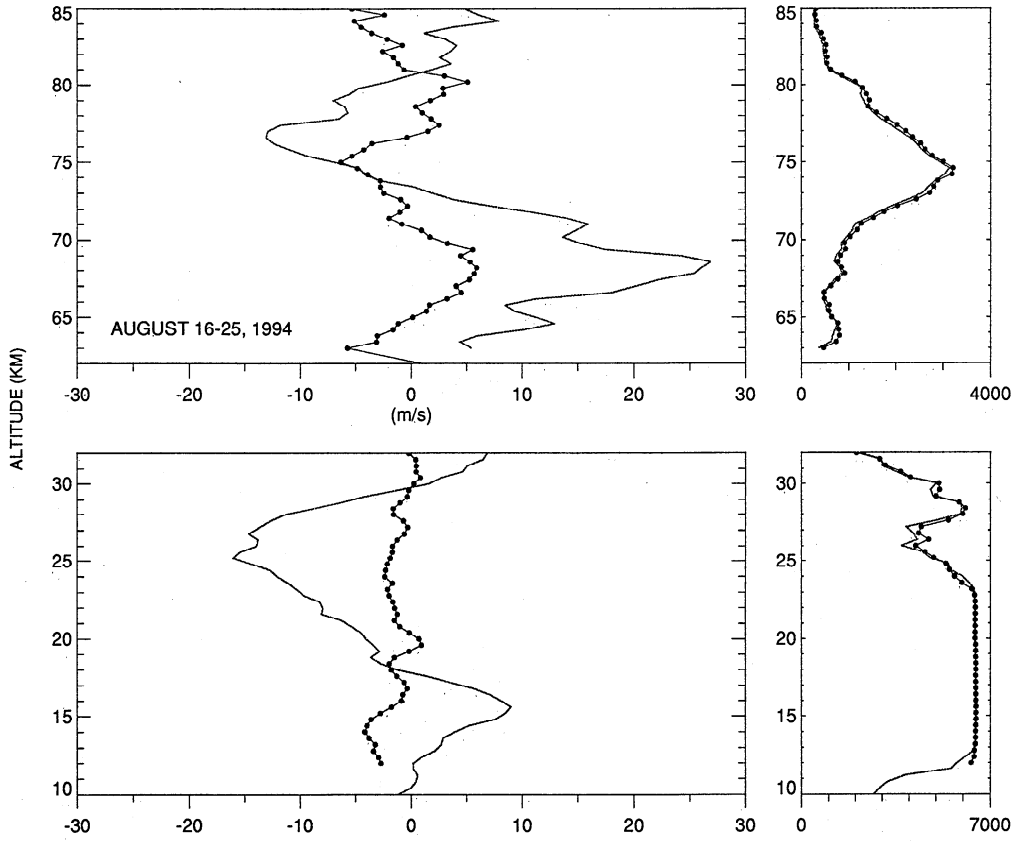

Figure 3. As in Figure 1 except for the period August 16-25, 1994. Note that the stratospheric profile extends down to 9.2 km.

count in the stratosphere and mesosphere for each of the three campaigns. Considerable variation among campaigns is observed for zonal wind profiles in both the stratosphere and mesosphere. It is perhaps surprising that in the mesosphere, meridional and zonal winds exhibit similar magnitudes and variability. These profiles cannot be understood in terms of a single phenomenon in each layer; the annual cycle and the QBO are both important in the stratosphere, while tides and the MSAO contribute in the mesosphere.

These wind estimates are averages of several hundred to several thousand observations. In the stratosphere the frequency of useful signal returns begins to decline quickly above ~30 km. In the August 1994 campaign there is an interesting secondary maximum in data count near 28 km (Figure 3). Similar secondary maxima in signal to noise ratio were found for the June and August 1987 campaigns at 32 and 30 km, respectively [cf. *Hitchman et al.* 1992, Figure 6]. All three maxima are located in strong vertical shear of the zonal wind and all occur during austral winter. This unexplained phenomenon may be caused by enhanced turbulence due to wave breaking or by significant gradients in temperature, humidity, or aerosol [*Hitchman et al.*, 1994].

Mesospheric data count profiles also exhibit interesting seasonal dependences. A pronounced maximum exists near 76 km in March 1994 (Figure 2) and 74 km in August 1994 (Figure 3), but the summer profile is quite different. In January 1993 the maximum occurs near 69 km, with a secondary maximum near 77 km. Since turbulent layers are required for a mesospheric signal return, this suggests that gravity wave breaking occurred at a lower level during January 1993 (southern summer).

3.2. Stratospheric Annual Cycle and QBO

Figure 1 of *Riggin et al.* [this issue] shows that the local ECMWF and JRO wind profiles agree rather well. In our calculations (not shown), differences between JRO and ECMWF winds interpolated to 12°S, 77°W are less than ~5 m/s throughout the stratosphere. This lends some support to the veracity of geographical features seen in the ECMWF analyses. In order to emphasize the significance of the annual cycle, we first show that the ECMWF zonal mean zonal winds over the equator are very different from wind behavior at JRO. The Singapore and Lima rawinsonde annual climatologies are chosen as pertinent examples of the geographical variation in the annual cycle. Finally, the horizontal and vertical structure of the subtropical monsoons is shown in synoptic charts for each campaign.

A time-altitude section of ECMWF stratospheric zonal mean zonal winds over the equator is shown in Figure 4. The vertical lines indicate central dates for the three CADRE campaigns. At the equator a robust QBO signal is seen, with QBO westerlies dominating in January 1993 and QBO easterlies dominating in March and Au-

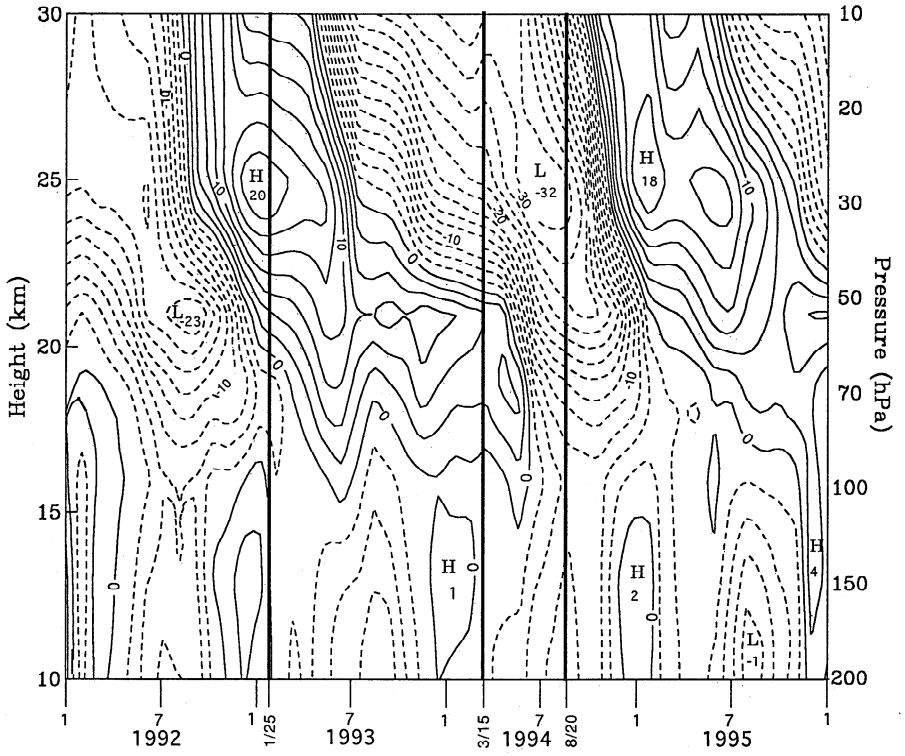

Figure 4. Time-altitude section of zonal mean zonal wind over the equator from ECMWF data, contour interval 2.5 m/s. Thick vertical lines indicate central times of the three JRO campaigns.

gust 1994. Climatologically, the QBO amplitude near 24 km exceeds 20 m/s over the equator and decreases to about 10 m/s near 12° latitude [e.g., *Andrews et al.*, 1987, Figure 8.2]. Thus one might expect a similar QBO variation over JRO but with about half the equatorial amplitude.

Even a cursory comparison between Figure 4 and Figures 1-3 reveals marked differences. Let JRO minus ECMWF zonally symmetric equatorial winds be denoted δU_{JE}. In January 1993, JRO winds are actually westward, while ECMWF equatorial winds are strongly eastward, with δU_{JE} peaking at -21 m/s near

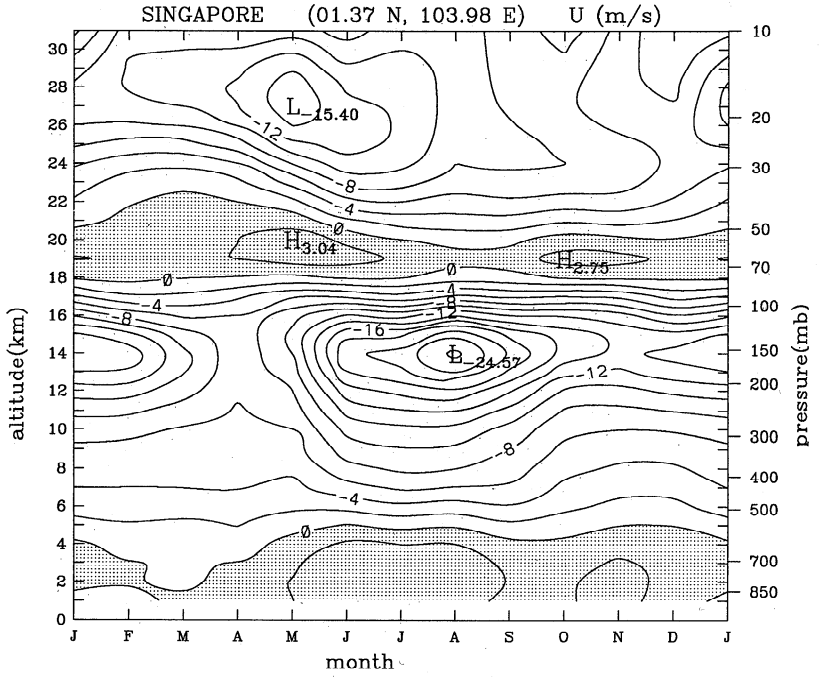

Figure 5. Time-altitude section of monthly averaged zonal wind at Singapore (1°N, 104°E) from ~34 years (1957-1990) of rawinsonde observations, contour interval 2 m/s, from *Yao* [1994].

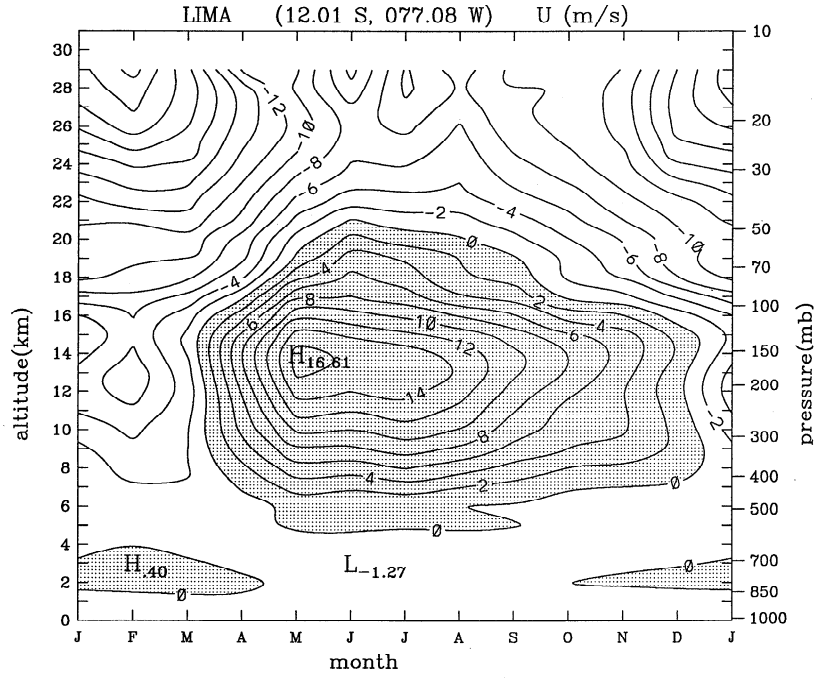

Figure 6. As in Figure 5, except at Lima (12°S, 77°W), from *Yao* [1994].

25 km. In March 1994, JRO winds are less westward than ECMWF, with δU_{JE} reaching +14 m/s near 30 km. In August 1994 during the QBO easterly maximum, JRO winds are much less westward, with δU_{JE} reaching +20 m/s near 30 km. Some of these differences are attributable to the zonally averaged seasonal behavior for southern hemisphere stations. Diminution of the QBO away from the equator must also be considered. Perhaps the least widely appreciated component of these differences is that there are significant climatological east-west variations of the annual cycle throughout the tropics and subtropics.

Yao [1994] showed that the annual cycle in zonal wind is quantitatively different at each of 15 widely spaced tropical stations. There is an accompanying spatial variation in temperature amplitude and, to a lesser extent, in the month of cold or warm maximum. Winds are a particularly sensitive indicator of this since they are a spatial gradient of the vertical integral of these temperature anomalies. Zonally asymmetric temperature structures are evanescent above the tropopause, but zonal wind structures are observed to at least 30 km, the top of radiosonde profiles. Although a separate manuscript is being prepared on this topic, Figures 5 and 6 give some indication of this phenomenon.

The climatological annual cycle in zonal wind at Singapore (1°N, 104°E, Figure 5) shows two upper tropospheric easterly maxima (-24 m/s in August and -15 m/s in January), weak westerlies all year near 19 km, with a complex seasonal cycle in the stratosphere: easterly flow peaks at -15 m/s near 27 km in April, with the easterly maximum occurring later at lower levels. The August easterly maximum in the upper troposphere is due to the proximity of the Asian subcontinent. This complex pattern is related to the underlying geography, with the time evolution being different for each station and for the equatorial zonal mean. Note that the stratospheric annual cycle at Singapore gives an easterly acceleration during March-August. This will tend to give the appearance of a more rapid descent of the QBO easterlies or stalling of QBO westerlies. This effect is more pronounced equatorward of the Tibetan High (see below), but may also be seen in the zonal mean (Figure 4). This is an alternative explanation for the clustering of "QBO easterly onset" seen over Singapore, Kwajalein, and Balboa (all northern hemisphere stations) in Figure 18 of *Dunkerton and Delisi* [1985].

The annual cycle at Lima (Figure 6) shows an upper tropospheric westerly maximum of 16 m/s near 14 km in May, while the stratospheric annual cycle has a peak easterly flow of -26 m/s near 30 km in February. Westerlies are expected in the southern winter near the tropopause due to the Hadley circulation. Note that the zero wind line in Figure 6 is near 20 km, well above the local tropopause at 16 km. The influence of the subtropical westerly jet extends appreciably into the stratosphere. These westerlies are strongest near Peru, being part of a trough which usually exists over the west coast of South America (cf. Figures 7a, 8a and 10a). The upward increase in the easterlies seen in January and the upward decrease in the westerlies seen in August associated with the annual cycle over Peru can explain most of the differences between Figures 1-3 and Figure 4. The JRO zonal wind profile in Figure 1 can be described as the superposition of summer easterly shear (Figure 6) and the QBO westerly maximum near 25 km (Figure 4), diminished in amplitude near 12°S. The JRO zonal wind profile in Figure 3 can be regarded as a superposition of the upward decreasing winter westerlies in August (Figure 6) with the QBO easterly shear (Figure 4).

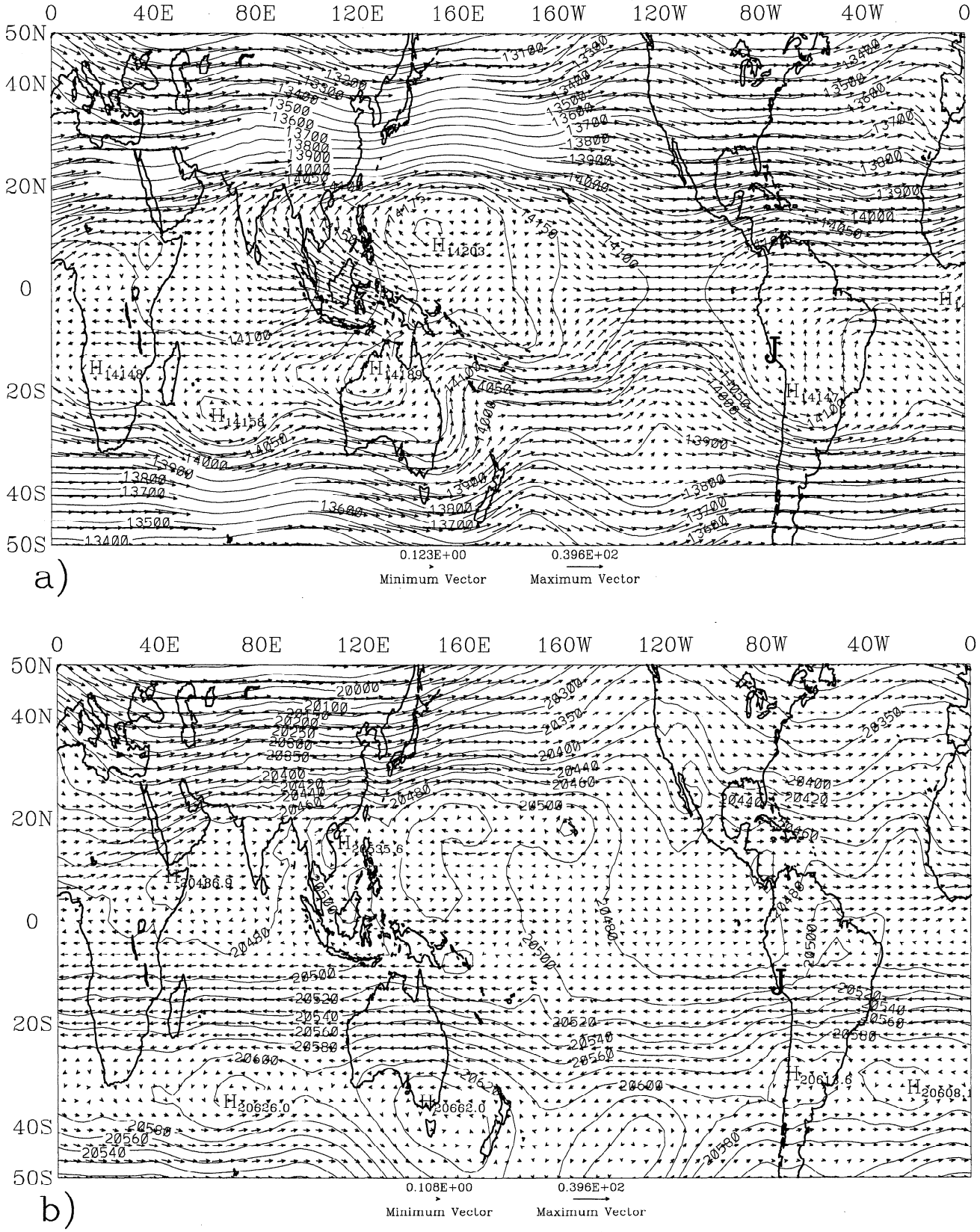

Figure 7. ECMWF geopotential heights and winds averaged for January 20-29, 1993, at (a) 150 hPa, contour interval 50 m, (b) 50 hPa, interval 20 m, (c) 30 hPa, interval 30 m, and (d) 10 hPa, interval 50 m. The maximum wind vector is 40 m/s. The location of JRO is designated with a J.

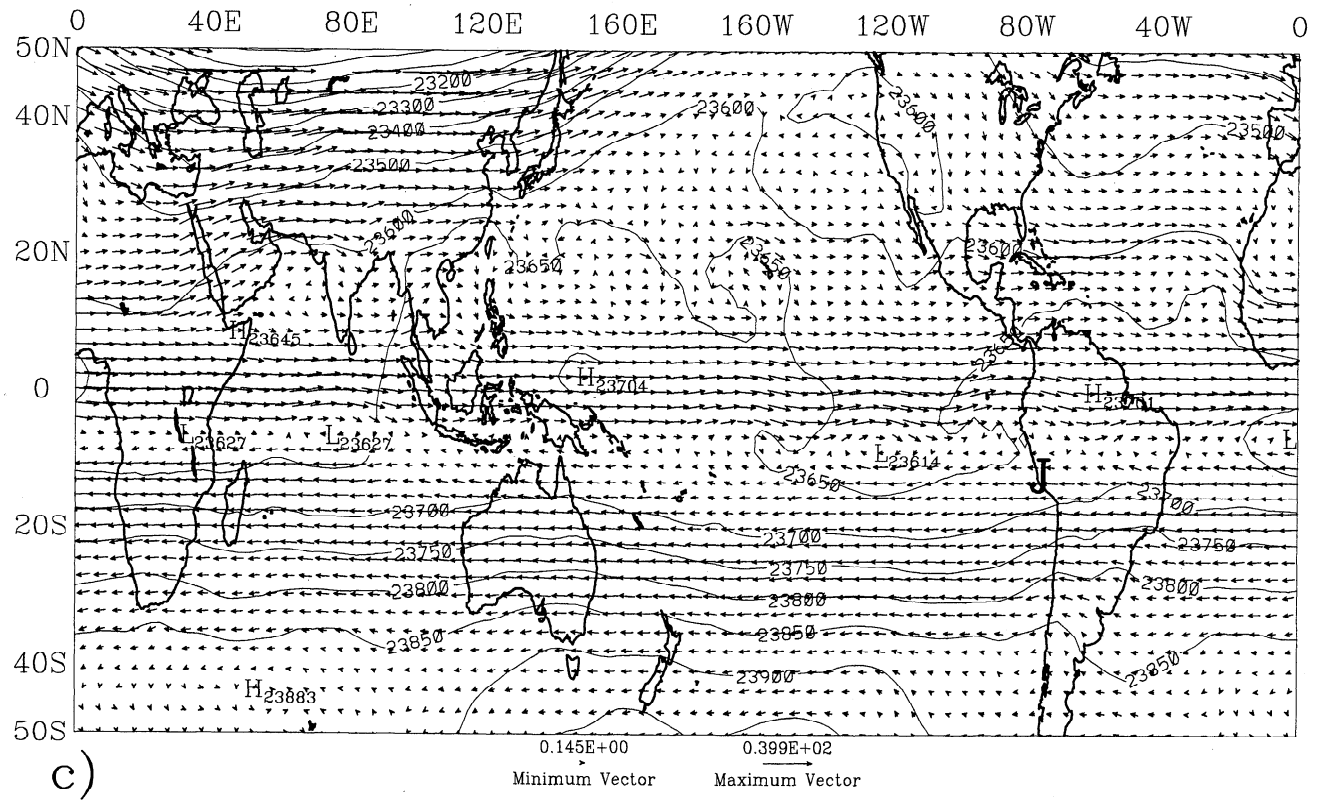

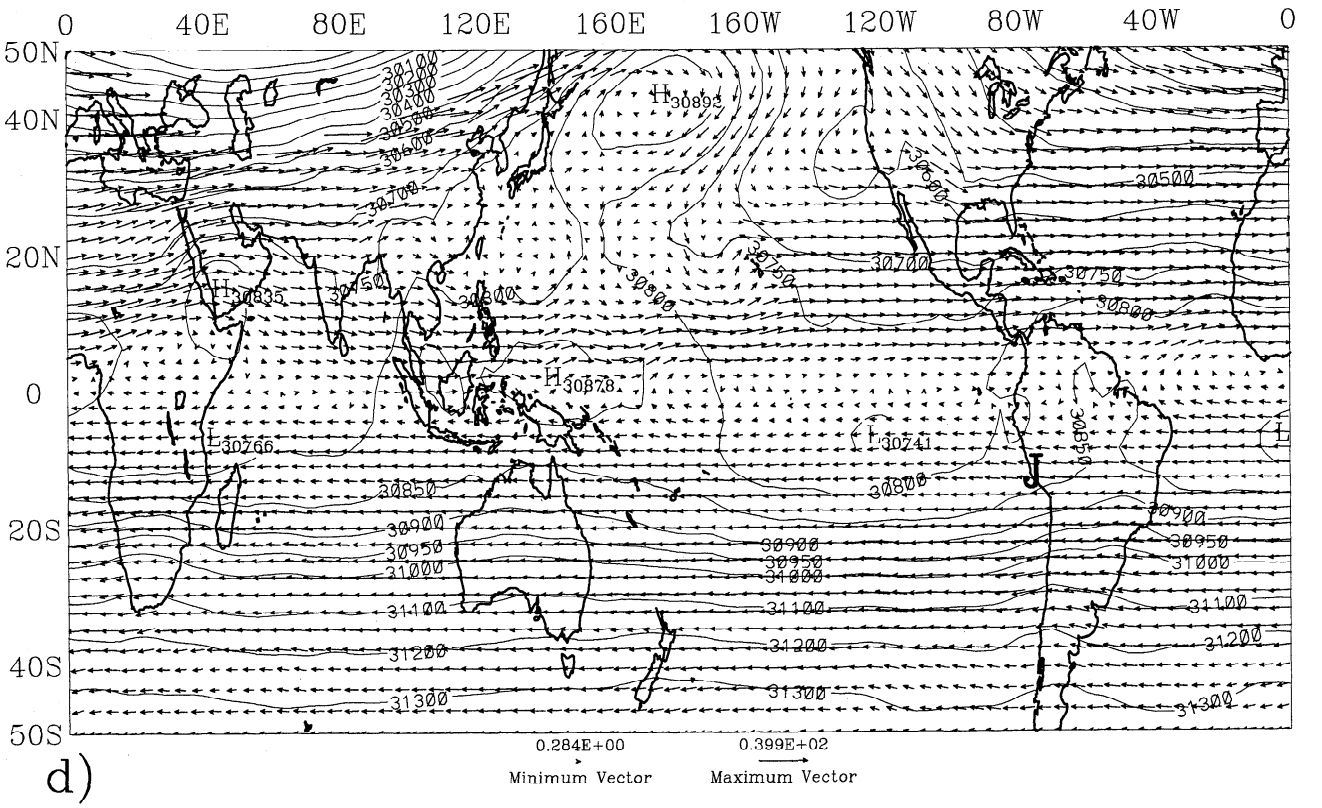

Figure 7. (continued)

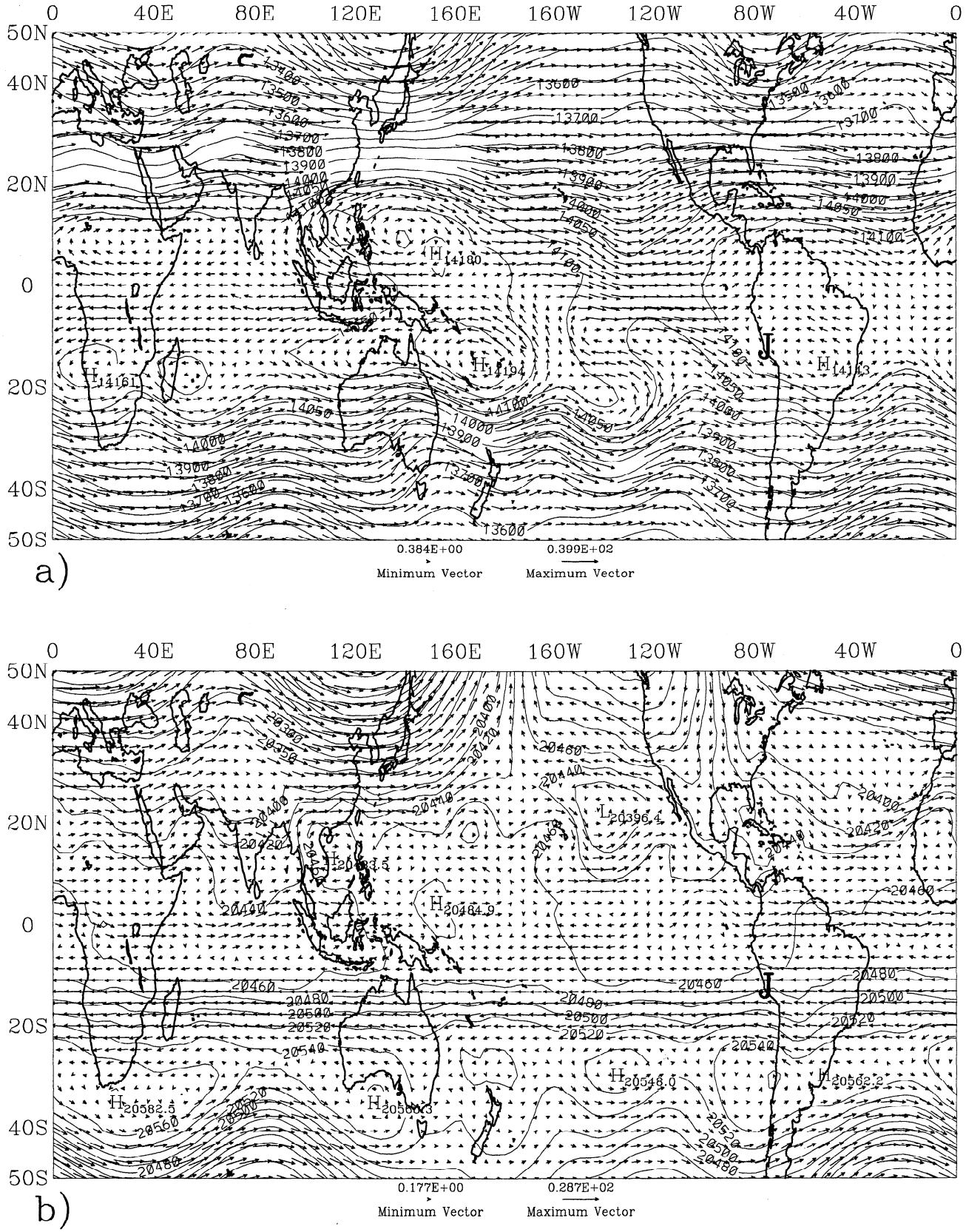

Figure 8. ECMWF geopotential heights and winds averaged for March 10-19, 1994, at (a) 150 hPa, contour interval 50 m, maximum wind vector of 40 m/s, and (b) 50 hPa, interval 20 m, maximum wind vector of 29 m/s.

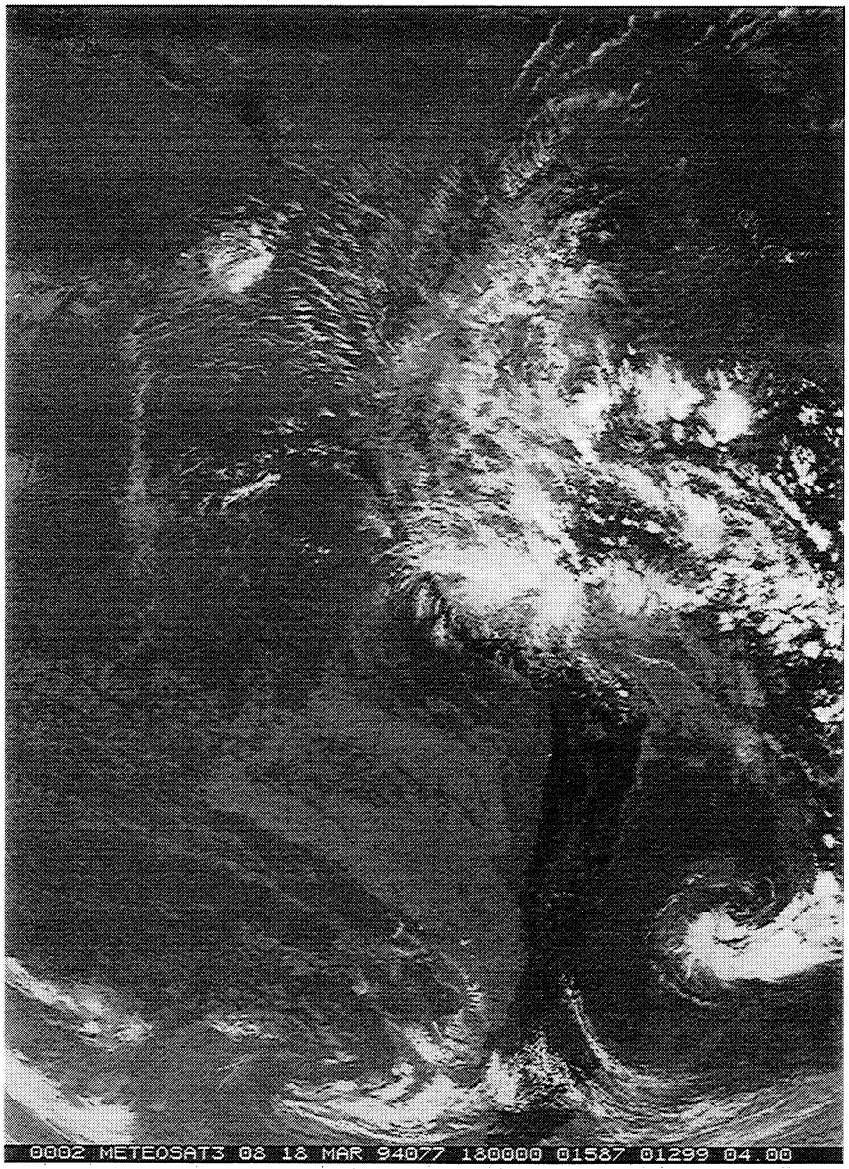

Figure 9. METEOSAT3 infrared image of tropical convection near JRO on March 18, 1994. The west coast of the Americas is seen in black near the center of the image, and high clouds are white.

Figures 7, 8, and 10 show ECMWF geopotential heights and winds at selected stratospheric pressure levels, averaged for each of the three campaigns. They reflect the influences of both the QBO and regionally varying annual cycle. The 150 hPa chart for the January 1993 campaign (Figure 7a) shows that during the southern summer, there are anticyclonic flows near the tropopause over South America, South Africa, and Australia [e.g., *Newell et al.*, 1972]. One may see that much of the northern winter Hadley circulation occurs near Southeast Asia. The anticyclone pair near Indonesia and eastward flow in the eastern Pacific have been described as a forced/damped westward extending mixed Rossby-gravity wave and eastward extending Kelvin wave [e.g., *Gill*, 1982], which may help explain the east Pacific trough. Note the easterly flow near 10°S across the Indian Ocean. Ascending in altitude, we find that the three southern summer anticyclones tilt poleward, merge zonally, and form the base of the subtropical easterly jet (Figures 7b-7d). At 50 hPa (~20.5 km) one sees modest easterly flow over JRO (Figure 7b), consistent with Figure 1. Note also the equatorward extension of the polar vortex in Figure 7b, with northeastward flow beginning near South America in the tropics, spiralling poleward across India into the North Pacific. This is an important pathway for material leaving the tropics and illustrates another kind of zonal asymmetry that can influence the tropics. Note the pathway for tropical air into the Aleutian High at 10 hPa in Figure 7d [cf. *Harvey and Hitchman*, 1996].

Figure 4 suggests that there are equatorial QBO westerlies beginning near 50 hPa during January 1993. In Figure 7b, however, equatorial easterlies exist east of Indonesia and from South America to Africa, but not at

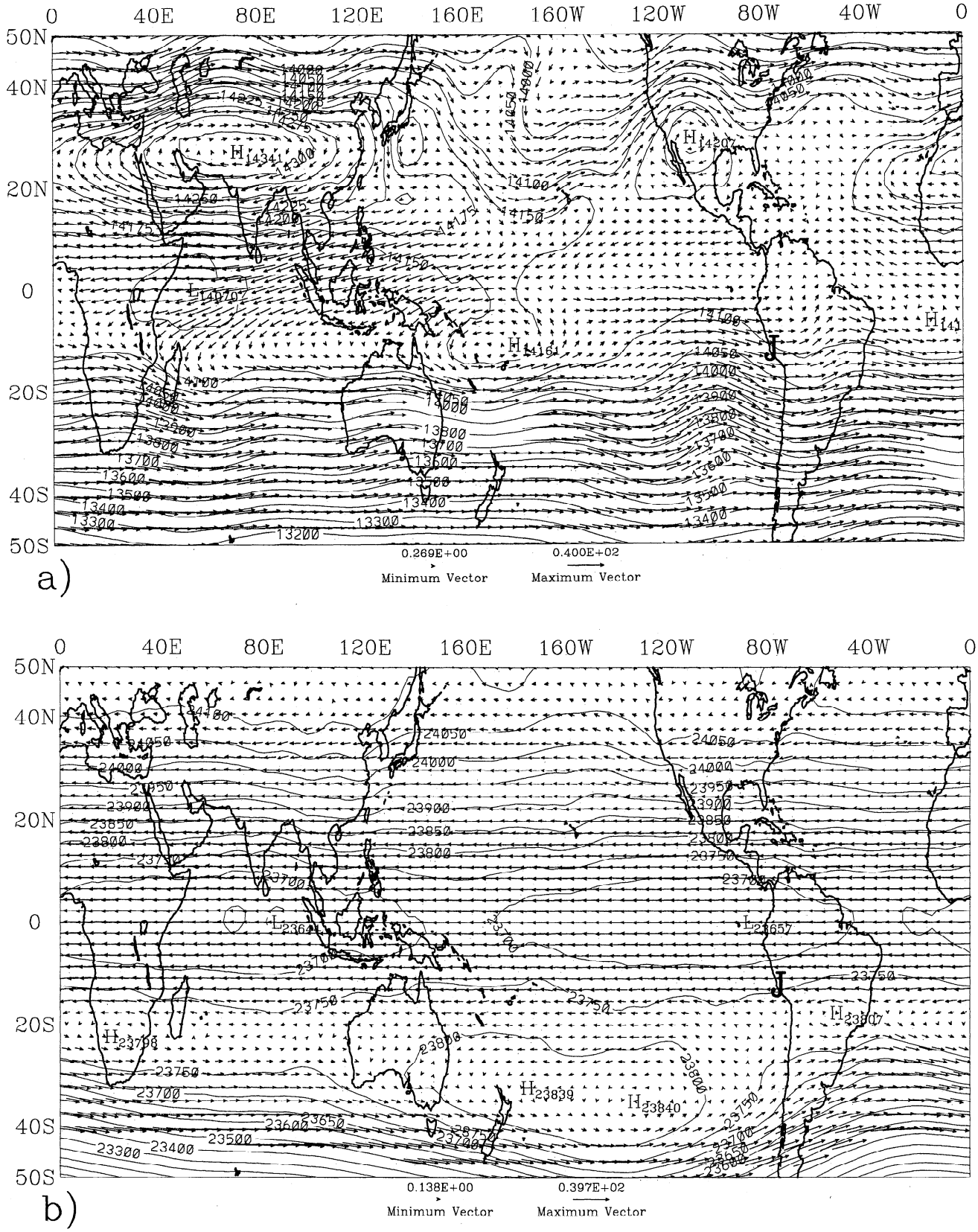

Figure 10. ECMWF geopotential heights and winds averaged for August 16-25, 1994, at (a) 150 hPa, (b) 30 hPa, and (c) 10 hPa. The contour interval is 50 m and maximum wind vector is 40 m/s.

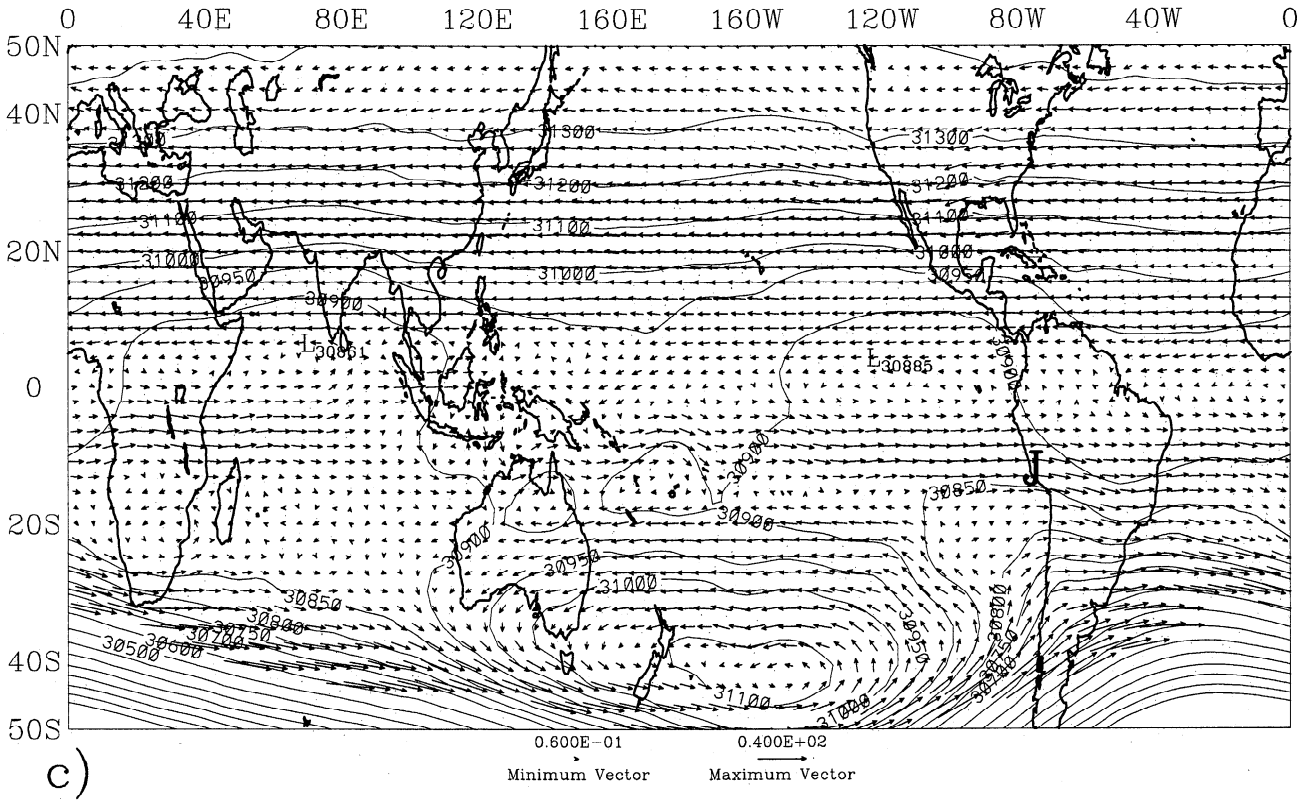

Figure 10. (continued)

other longitudes. One might regard this pattern as the base of the descending QBO westerlies having a long undulation on it caused by monsoon and winter planetary wave patterns. At 30 hPa (~24 km) the QBO westerly regime can clearly be seen between the summer easterlies and winter longwave pattern (Figure 7c). Both JRO and local ECMWF winds are slightly easterly at 30 hPa (Figures 1 and 7c). In Figure 4 equatorial zonal mean ECMWF winds are still westerly near 30 km, but the 10 hPa (~31 km) chart (Figure 7d) suggests that the zonal mean QBO westerlies near 30 km are an average of zonally-varying winds. The substantial summer subtropical easterly flow over JRO at this level is also verified (Figure 1). A salient feature of Figures 7a-7d is the structure of the southern summer anticyclones, which tilt poleward and merge zonally with increasing altitude. This structure in geopotential height geostrophically underlies the summer easterly jet, which exists equatorward of the anticyclones. Increasing with altitude, this easterly jet dominates the summer flow to ~5°S (Figure 7d).

The 150 hPa chart for the March 1994 campaign (Figure 8a) shows that three continental anticyclones are still located south of the equator approaching the equinox. This lag of the subsolar point is likely due to the thermal inertia of the underlying continents and oceans. Daily METEOSAT images (e.g., Figure 9) depict intense convection in association with the South American anticyclone at this time. One may see the influence of divergent outflow from the extensive area of convection on the wind and height patterns in Figure 8a. As in the January 1993 campaign, the continental anticyclones tilt poleward with altitude and merge zonally, yielding an upward intensifying subtropical easterly jet on the equatorward side (Figure 8b). Over JRO, weak easterly flow is seen near 50 hPa (~20.5 km) (Figure 2). Figure 4 suggests that QBO westerlies are present over the equator near 50 hPa, but in Figure 8b the top of the QBO westerly layer appears quite narrow and zonally varying. Above this level, the equatorial QBO easterlies and the southern subtropical easterlies over JRO both increase with altitude. Thus the easterlies which increase with height in both Figures 2 and 4 are due to distinctly different phenomena at the two locations: QBO easterlies over the equator and spring subtropical easterlies over JRO (compare Figure 6).

The 150 hPa chart (~14 km) for the August 1994 campaign (Figure 10a) illustrates the tremendous influence of the Tibetan High on the eastern hemisphere tropics. The upper tropospheric Hadley circulation occurs almost entirely near the Indian Ocean. Note the marked cross-equatorial flow into the winter hemisphere over the Indian Ocean. Owing to the resulting poleward deformation of the southern winter westerly jet in the eastern hemisphere, the equatorward influence of the southern winter westerlies is largest off the coast of South America. This trough caused a west-northwesterly flow over JRO at 14 km (Figure 3). In most winters, winds gradually become moderately easterly into the stratosphere over Lima (Figure 6), but this particular August had strong QBO easterlies, peaking at 25 km over the equator (Figure 4). In Figure 10b one

can see that JRO is under the influence of QBO easterly flow, consistent with the -17 m/s westward maximum near 25 km in Figure 3. This 30 hPa chart shows strong easterly flow throughout the band 20°S-40°N. At these heights the subtropical northern summer easterlies blend continuously with the tropical QBO easterlies. The flow at 10 hPa (~31 km) near JRO is westerly, markedly different from that at 30 hPa (Figures 3, 10b, and 10c). A large zonal wavenumber one disturbance is evident poleward of 20°S, with weak flow near 20°S. A separate band of westerlies is centered near 12°S (cf. Figure 3). Figure 4 shows that during August 1994 QBO westerlies are approaching the 30 km level over the equator. If Figure 10c has some validity, it is possible that the leading edge of the descending QBO westerlies is appearing near 12°S in this month. This might be expected, given that the northern summer easterly jet has significant amplitude at the equator (Figure 5).

3.3. Mesospheric SAO and Diurnal Tide

Considerable mesospheric variability is seen in both wind components in Figures 1-3. We consider contributions from both the MSAO and the diurnal tide. Some guidance for interpreting JRO mesospheric winds in terms of the diurnal tide is given by *Hays et al.* [1994] and *Burrage et al.* [1995a], who compared HRDI diurnal tidal amplitudes with results from a global model. They showed that diurnal tide meridional wind amplitudes near 12° latitude exceed 20 m/s near 80-85 km, while zonal winds amplitudes are much smaller. *Burrage et al.* [1995b] studied the semidiurnal tide in HRDI data and showed it to be significantly smaller than the diurnal tide near 12°S. It should be noted that the diurnal tide probably contributes toward some of the zonal wind signal in Figures 1-3, but a quantitative assessment of the relative contributions by the diurnal tide and MSAO would require other information.

Zonal winds in Figures 1-3 suggest time mean westerlies near 65-70 km and time mean easterlies near 75-80 km, consistent with previous observations [e.g., *Cole*, 1968; *Groves*, 1972]. Observations of the MSAO in zonal wind include studies using rockets [*Hirota*, 1978; *Hamilton*, 1982], temperatures from the Solar Mesosphere Explorer [*Garcia and Clancy*, 1990], meteor echo radars [*Avery et al.*, 1989], MF partial reflection radar [*Vincent and Lesicar*, 1991], and HRDI observations [*Lieberman et al.*, 1993; *Hays et al.*, 1994]. The general picture that emerges is one of wind regimes descending at a rate of perhaps 10 km/month, but with considerable interannual variability. Since gravity wave drag is a primary component of the MSAO, it is likely that the annual cycle, stratopause SAO, and QBO would modulate gravity wave transmission and hence the strength of a particular MSAO cycle [*Delisi and Dunkerton*, 1988]. Moreover, large day to day variability at JRO tends to obscure any descent that might be occurring in basic state winds. An irregular descending pattern does emerge if one considers the January-August-March samples as a 3 month sequence in a semiannual harmonic: westerly maxima are found near 74 km in January 1993, 73 km in August 1994 and 66 km in March 1994, while easterly maxima are found near 85 km in January 1993, 76 km in August 1994, and 75 km in March 1994 (Figures 1-3). August 1987, however, showed a strong east-

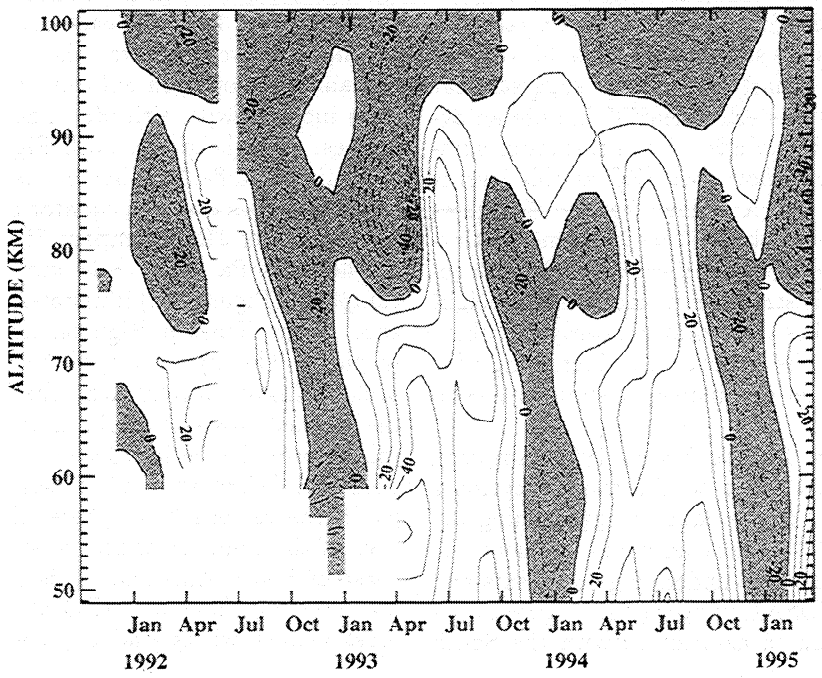

Figure 11. Time altitude section of monthly and zonally averaged HRDI zonal winds at 12°S, contour interval 10 m/s.

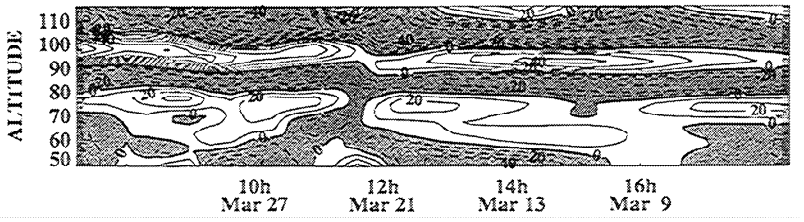

Figure 12. Time altitude section of HRDI meridional winds near 12°S, 77°W for March 1994, contour interval 10 m/s. Note that the local crossing time varied during this period.

erly maximum near 70 km [*Hitchman et al.*, 1992, Figure 2], while westerlies were found at that level in August 1994.

This rather difficult picture is clarified considerably by examining a time altitude section of monthly and zonally averaged HRDI zonal winds near 12°S (Figure 11). A similar figure was shown by *Lieberman and Hays* [1994] but for the equator and ending in May 1993. A comparison of Figure 11 with Lieberman and Hays' Figure 12 reveals that significant differences exist between 12°S and the equator in the mesosphere. Although considerable variability is seen from cycle to cycle for the MSAO, regular downward progression of wind regimes is evident. Zonal mean HRDI and JRO zonal winds both show a 10 m/s westerly maximum near 70-75 km and a -20 m/s easterly maximum near 85 km in January 1993, a 10 m/s westerly maximum near 67 km and a -10 m/s maximum near 80 km in March 1994, and westerlies exceeding 20 m/s near 68 km in August 1994. Above 68 km in August 1994, both show easterly shear, but JRO shows a 77 km easterly maximum of -15 m/s, which is stronger than in the HRDI section. Despite the different vertical resolutions of 400 m for JRO and ~5 km for HRDI and the possibility of significant east-west variations, JRO and HRDI zonal winds agree remarkably well in the tropical mesosphere.

Mesospheric meridional winds are nearly as large as zonal winds at JRO, and the flow is not simply from the summer to winter hemisphere (Figures 1-3). In January 1993 southward flow (toward the summer hemisphere) of -22 m/s maximizes near 84 km. A similar -12 m/s southward flow is seen near 82 km in March. In August 1994 northward flow maxima are seen near 68 and 80 km, with southward flow near 75 km. Theoretical estimates of zonal mean meridional flows implied by the seasonal or MSAO changes in zonal flows do not exceed a few meters per second [e.g., *Holton* 1983; *Hitchman and Leovy* 1986; and section 4]. Given that HRDI and JRO zonal winds agree, it is likely that the substantial JRO meridional winds represent geophysical phenemona. For example, *Fritts et al.* [this issue] describe a large amplitude 2-day wave event in the mesosphere during January 1993.

Since JRO sampled daily for 10 hours centered around noon, a campaign mean profile should contain a diurnal tide signal, with a noon maximum signal being damped by $\sim 2/\pi$. Although the semidiurnal tide is not negligible at JRO [*Fritts et al.*, 1992], 10 hour averaging should result in only a very small residual for the semidiurnal tide. Figure 12 shows HRDI meridional winds near JRO during March 1994. Later local satellite sampling times occurred earlier in the month. Meridional winds exhibit downward progression and a 20-25 km vertical wavelength near 80 km, behaving in a manner consistent with the diurnal tide. There is a broad agreement between Figures 2 and 12, with southward flow near 83 km and northward flow near 72 km. We conclude that the diurnal tide is probably responsible for much of the structure in meridional wind seen in Figures 1-3.

4. Vertical Motions and Momentum Fluxes

Figures 13-15 show the vertical winds for each campaign. The north-south and east-west beam pair estimates agree very well in the mesosphere and moderately well in the stratosphere. During August 1994

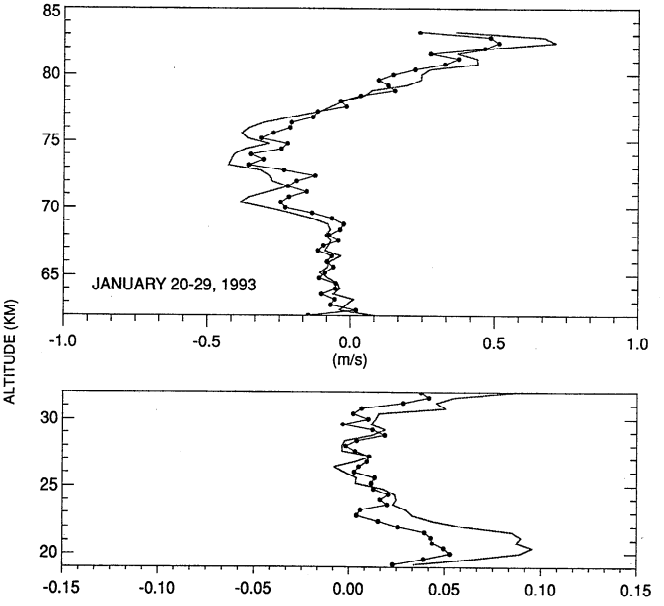

Figure 13. Campaign average vertical wind at JRO (12°S, 77°W) estimated from the east-west beam pair (thin line) and north-south beam pair (thin line with dots) during January 20-29, 1993. The speed range in the mesosphere is ±1.0 m/s, while that in the stratosphere is ±15 cm/s.

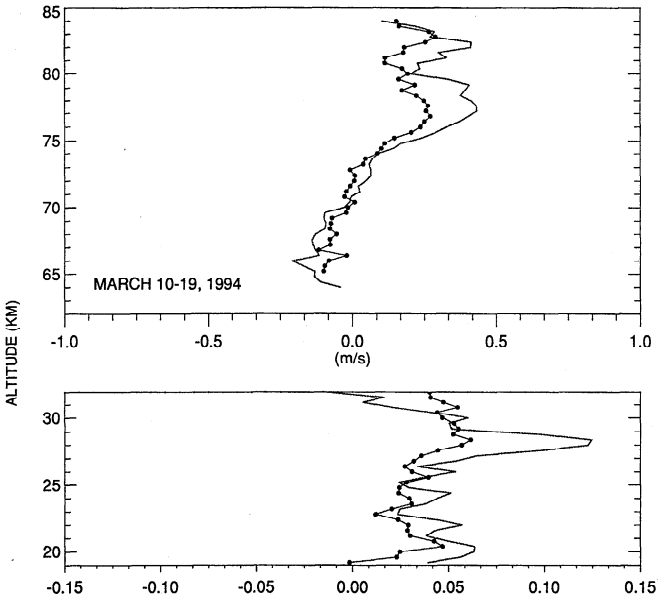

Figure 14. As in Figure 13 except for the period March 10-19, 1994.

the two beam pairs depict different vertical structures in the stratosphere. The correlation coefficient for profiles of w_{ew} and w_{ns}, averaged for all of the campaigns, exceeds 0.9 in the mesosphere and is ~0.4 in the stratosphere. The good agreement in the mesosphere confirms the lack of beam pointing errors and provides a powerful constraint on the nature of the vertical motions. For these CADRE campaigns, mesospheric magnitudes are ~10-50 cm/s, while stratospheric magnitudes are ~1-5 cm/s, similar to magnitudes found in our 1987 campaigns [*Hitchman et al.*, 1992] and in special observations of vertical motions at JRO by *Maekawa et al.* [1993].

By considering the approximate balance $\overline{w}\,\overline{\theta}_z \approx \overline{Q} \approx -\delta\overline{\theta}/\tau_{\rm rad}$ it becomes clear that these motions are much too large for zonally symmetric phenomena such as the MSAO or QBO. If one assumes a mesospheric temperature perturbation $\delta\overline{\theta}$ ~10 K, with a radiative damping time scale $\tau_{\rm rad}$ ~2 days, vertical motions should be less than 5 mm/s. A stratospheric 5 K perturbation with a 10 day timescale suggests stratospheric vertical motions of less than ~0.5 mm/s. An interactive two dimensional model of the QBO with a detailed radiative heating algorithm suggests vertical motion maxima of ~0.3 mm/s [*Politowicz and Hitchman*, 1997]. Furthermore, for most of the JRO data, $|v|/|w| << 100 << N/f$ (Prandtl's ratio, which approximates the aspect ratio of large-scale circulations). An alternative explanation must be sought to explain the large vertical motions.

It is of interest to first address the remarkable anticorrelation between horizontal and vertical winds found for features with vertical scales exceeding ~2 km, especially in the mesosphere (compare Figures 1-3 and 13-15). In January 1993, near 75 km northeastward flow of ~10 m/s occurs where there is descent of ~30 cm/s, while near 85 km southwestward flow of ~25 m/s occurs where there is ascent of ~50 cm/s. In March 1994, near 77-82 km, westward flow of ~12 m/s occurs with ~40 cm/s ascent, while near 65 km, eastward flow of ~8 m/s coincides with descent of ~10 cm/s. In August 1994, the flow is east-northeastward and downward near 68 km; southwestward and upward near 75 km; and southeastward and downward near 84 km. In the stratosphere, upward and westward motions tend to occur together. The correlation coefficient for profiles of u and w_{ew} and of u and w_{ns}, averaged for beam pairs and all of the campaigns, is ~-0.5 in the mesosphere and is ~-0.4 in the stratosphere. Horizontal-vertical wind covariances for the time averaged flow often exceed 1 $m^2\ s^{-2}$, contributing significantly to total momentum fluxes.

Any explanation for these large vertical motions must satisfy the two observational constraints of north-south and east-west beam pair agreement and anticorrelation with zonal wind. Consider aspect sensitivity as a possible explanation [*Kudeki et al.*, 1990, 1993]. Assume a thin turbulent layer tilted at angle δ with respect to the horizontal, where a positive value indicates upward toward the east. Backscatter would be received most strongly from an angle of $\theta - \delta$ for the beam looking in the upward tilted direction, and from an angle of $\theta + \delta$ for the beam looking in the downward tilted direction. Then for a pure zonal flow u, the line-of-sight radial velocity seen in the west beam would be $U_w = -u\sin(\theta+\delta)$ and in the east beam it would be $U_e = u\sin(\theta-\delta)$. Inserting these in (1a) and (2a) and assuming $|\delta| << |\theta| << 1$, one obtains $u_{ew} \approx u$

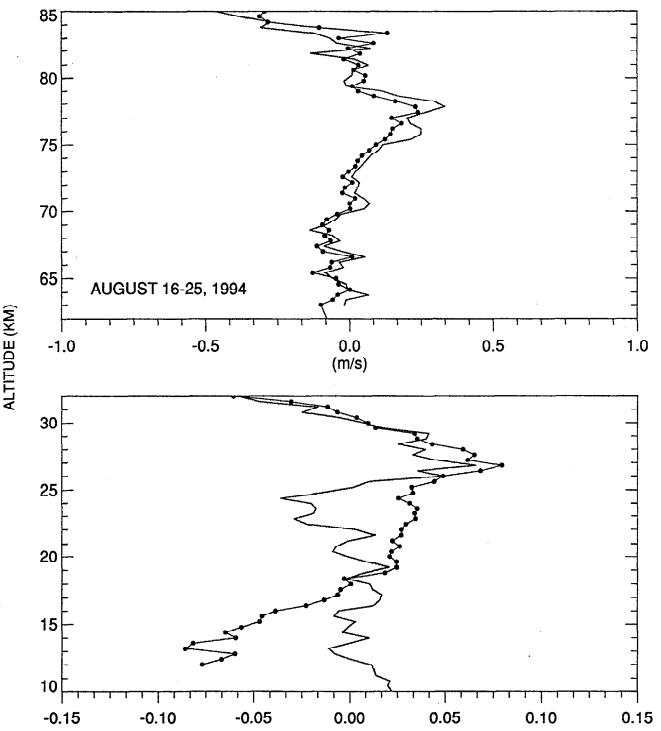

Figure 15. As in Figure 13 except for the period August 16-25, 1994. Note that the stratospheric profile extends down to 9.2 km.

and $w_{ew} \approx -u\ \delta$. Due to the finite azimuthal beam width, a purely zonal flow u could have a similar effect on the north-south beam pair, where backscatter would be received most strongly from an angle δ toward the downward tilted direction of the turbulent layer. The line-of-sight velocity in the south beam would then be $U_s = -u \sin(\delta)$ and in the north beam it would be $U_n = u \sin(-\delta)$. Inserting these in (1b) and (2b), one obtains $v_{ns} \approx 0$ and $w_{ns} \approx -u\ \delta$. For $u/w \sim$ -100 to -400, $\delta \sim +0.6°$ to 0.1°, implying a chronic upward tilt toward the east for turbulent layers.

Any possible explanation for these vertical motions requires consideration of processes at a smaller scale than the zonal mean. In the mesosphere, tides may contribute to the vertical motion pattern. From the continuity equation, assuming vertical and meridional half wavelengths of 12 km and 12° and a characteristic meridional motion magnitude of 20 m/s, vertical motions of about 20 cm/s could occur in association with the diurnal tide. Since temperature amplitudes increase with altitude for the diurnal tide, the phase relationship between meridional and vertical motion should vary with altitude. A possible interpretation of mesospheric vertical winds at JRO is that broad equatorial updrafts occur where the tidal meridional wind is convergent; downdrafts occur with divergence. The anticorrelation between u and w in the mesosphere may represent the upward flux of easterly momentum by the diurnal tide.

A variety of Stokes' drift may be relevant to this problem. This possibility was discussed by *Coy et al.* [1986] as an explanation of large mesospheric subsidences ob-

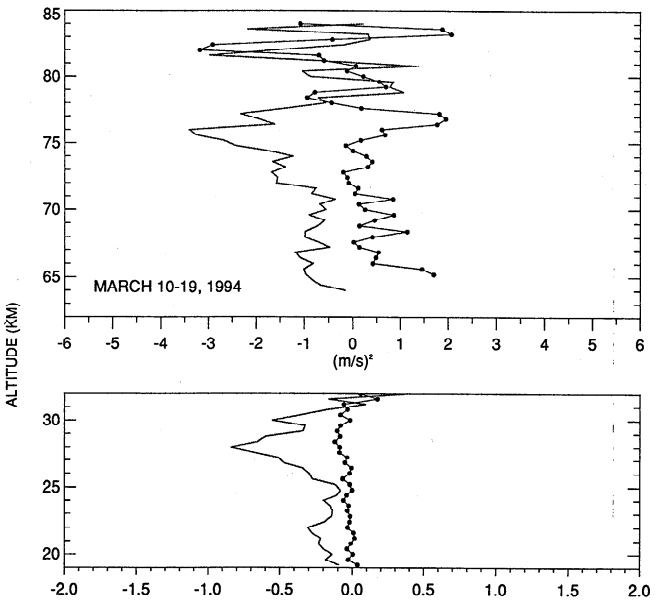

Figure 16. Campaign average horizontal-vertical wind covariances at JRO (12°S, 77°W): $\overline{uw}$ estimated from the east-west beam pair (thin line) and $\overline{vw}$ estimated from the north-south beam pair (thin solid with dots) during March 10-19, 1994. The range in the mesosphere is ± 6 m^2 s^{-2} and in the stratosphere is ± 2 m^2 s^{-2}.

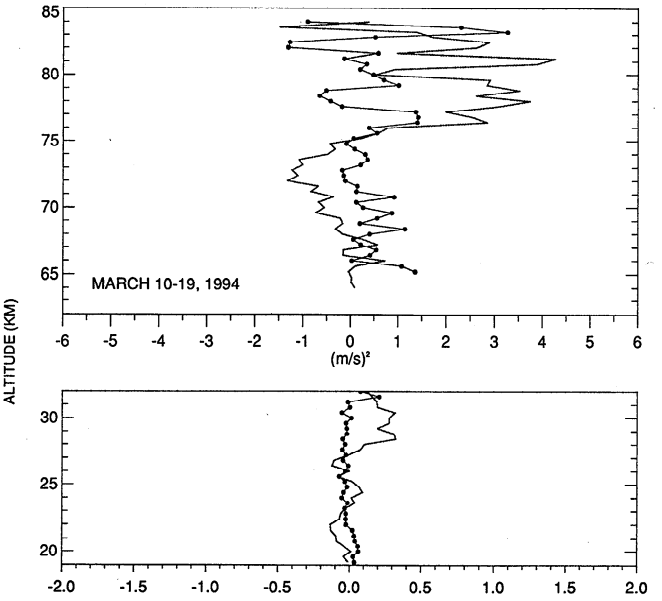

Figure 17. As in Figure 16, except for the eddy momentum fluxes ($\overline{u'w'}$, $\overline{v'w'}$).

served over Poker Flat, Alaska, during boreal summer [*Balsley and Riddle*, 1984]. It is also possible that radar reflectivity is sampling a moving pattern of turbulence. Surface waves on the ocean generate foam visible to the eye via scattering of visible sunlight in a pattern which forms at the crest and descends with time as it subsides. Gravity wave breaking may similarly generate patterns of ascending or descending turbulent patches, which would manifest a Doppler shift in the returned radar signal. Since breaking gravity waves tend to occur in a sawtooth pattern for potential temperature, aspect sensitivity could introduce a bias regarding which phase of the wave is most strongly represented in the return signal. *Cornish* [1988], and *Hoppe and Fritts* [1995] describe further aspects of interpretating large vertical motions sensed by radar.

For the August 1994 campaign it is possible that a significant standing wave pattern existed in the stratosphere. If so, it would require a chronic horizontal length scale comparable to the beam pair separation (~2 km near 20 km altitude). This period was distinguished by a large-amplitude trough/ridge pair that occupied the troposphere and lower stratosphere (Figures 10a and 10b), with substantial northeasterly flow near 5 km. It is conceivable that this generated a mountain wave which caused the differences between w_{ew} and w_{ns}.

Ambiguity in the physical meaning of large time mean vertical motions leads to ambiguity in the interpretation of momentum fluxes. As an example of this difficulty, the March 1994 campaign mean momentum fluxes for the total ($\overline{uw}$, $\overline{vw}$), eddy ($\overline{u'w'}$, $\overline{v'w'}$), and mean winds or "DC signal" ($\overline{u}\ \overline{w}$, $\overline{v}\ \overline{w}$) are shown in Figures 16-18. Velocity covariances in Figure 16 are ~1-3 m^2 s^{-2} in the mesosphere and ~0.1-1.0 m^2 s^{-2} in the stratosphere. Zonal fluxes tend to be westward in both the strato-

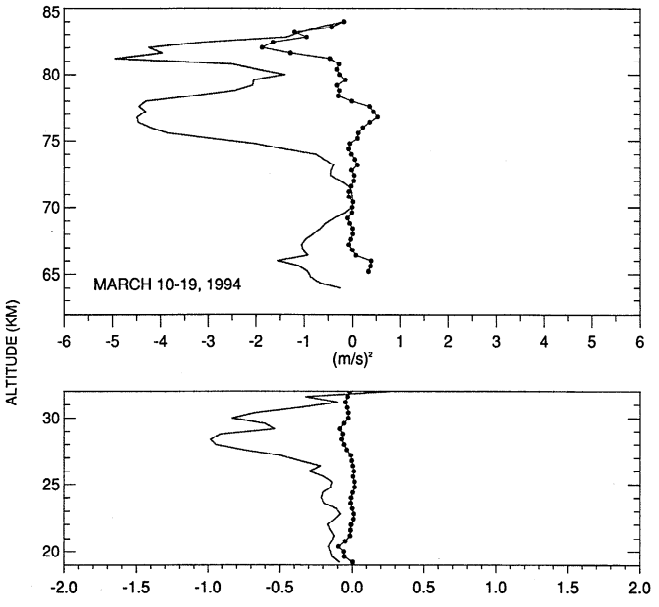

Figure 18. As in Figure 16, except for fluxes by the time mean winds ($\overline{u}\ \overline{w}$, $\overline{v}\ \overline{w}$).

sphere and mesosphere. Meridional fluxes tend to be smaller, but significant northward fluxes are seen in the mesosphere. Fluxes associated with the "mean winds" (Figure 18) are often larger than the "eddy fluxes" (Figure 17). This presents a challenge in interpreting radar momentum fluxes in general.

5. Summary and Conclusions

These three JRO campaigns sampled the stratospheric and mesospheric winds at distinct phases of the annual cycle, QBO, SAO, and so provide a useful contribution to the wide variety of observations used to establish a climatology of the tropical middle atmosphere. The general agreement for horizontal winds between ECMWF and JRO in the stratosphere and between HRDI and JRO in the mesosphere tends to support the fidelity of coherent features found in these data sets. To understand the evolution of the tropical stratospheric flow, it is essential to take account of the complex interaction between the geographically varying annual cycle and the QBO. This is particularly important for diagnosing tracer transport between the stratosphere and troposphere and between the tropics and extratropics. To understand the evolution of the tropical mesospheric flow, it is essential to consider both the MSAO and the tides. Although the MSAO may dominate zonal winds and the diurnal tide may dominate meridional winds near 12° latitude, further work is warranted to deconvolve the two phenomena. This presents a challenge for theoretical interpretation of meridional circulations in the tropical mesosphere.

The chronically large vertical motions are also an intriguing challenge. In the mesosphere they may represent tidal motions. The anticorrelation between vertical and horizontal winds, together with aspect sensitivity arguments, may suggest a chronic eastward tilting of turbulent layers. In March 1994, vertical motions of ~4 cm/s existed in the stratosphere (Figure 14). The METEOSAT image of Figure 9 reveals the intense convection which occurred just east of JRO during March. It is not known precisely how air enters the stratosphere and ascends near convection [*Newell and Gould-Stewart*, 1981]. Ascent may involve a type of gravity wave-induced Stokes' drift. Understanding radar vertical motions may lend insight into this process. Since the mean winds contribute substantially to the total momentum fluxes, this problem must also be solved in order to utilize radar-derived momentum fluxes in diagnosing the momentum budget of the tropical middle atmosphere.

Acknowledgments. We would like to acknowledge conversations with Manabu Yamanaka, Kaoru Sato, Takuji Nakamura, Ron Woodman, and Adrian Tuck. We also acknowledge the support of NSF grants ATM-9120110, ATM-9118899, and ATM-9214657, NASA grants NAS1-19958, SASS-94-009, NAG5-2722, and NAG5-2806. We used facilities at the JRO and National Center for Atmospheric Research (NCAR) during the course of this work. JRO and NCAR are funded by the National Science Foundation.

References

Andrews, D. G., J. R. Holton, and C. B. Leovy, *Middle Atmosphere Dynamics*, 489 pp., Academic, San Diego, Calif., 1987.

Avery, S. K., R. L. Obert, and J. P. Avery, Observations of equatorial mesospheric mean winds and tides, in *Handbook for Middle Atmosphere Program*, SCOSTEP Secretariat, *28*, 64-67, 1989.

Balsley, B. B., and A. C. Riddle, Monthly mean values of the mesospheric wind field over Poker Flat, Alaska. *J. Atmos. Sci.*, *41*, 2368-2700, 1984.

Bergman, J. W., and M. L. Salby, Equatorial wave activity derived from fluctuations in observed convection, *J. Atmos. Sci.*, *51*, 3791-3806, 1994.

Bjerknes, V., J. Bjerknes, T. Bergeron, and H. Solberg, *Physikalische Hydrodynamik*, 797 pp., Springer-Verlag, New York, 1933.

Burrage, M. D., M. E. Hagan, W. R. Skinner, D. L. Wu, and P. B. Hays, Long-term variability in the solar diurnal tide observed by HRDI and simulated by the GSWM, *Geophys. Res. Lett.*, *22*, 2641-2644, 1995a.

Burrage, M. D., D. L. Wu, W. R. Skinner, D. A. Ortland, and P. B. Hays, Latitude and seasonal dependence of the semidiurnal tide observed by the high-resolution Doppler imager, *J. Geophys. Res.*, *100*, 11,313-11,321, 1995b.

Chen, P., Isentropic cross-tropopause mass exchange in the extratropics, *J. Geophys. Res.*, *100*, 16,661-16,673, 1995.

Cole, A. E., Periodic oscillations in the tropical and subtropical atmosphere at levels between 25 and 80 km, *Space Res.*, *8*, 823-834, 1968.

Cornish, C. R., Observations of vertical velocities in the tropical upper troposphere and lower stratosphere using the Arecibo 430-MHz radar, *J. Geophys. Res.*, *93*, 9419-9431, 1988.

Coy, L., D. C. Fritts and J. Weinstock, The Stokes drift due to vertically propagating internal gravity waves in a compressible atmosphere, *J. Atmos. Sci.*, *43*, 2636-2643, 1986.

Delisi, D. P., and T. J. Dunkerton, Seasonal variation of

the semiannual oscillation, *J. Atmos. Sci.*, *45*, 2772-2787, 1988.

Dove, H. W., *Meteorologische Untersuchungen*, 344pp., Sandersche Buchhandlung, Berlin, 1837.

Dunkerton, T. J., Theory of the mesopause semiannual oscillation, *J. Atmos. Sci.*, *39*, 2681-2690, 1982.

Dunkerton, T. J., Evidence of meridional motion in the summer lower stratosphere adjacent to monsoon regions, *J. Geophys. Res.*, *100*, 16,675-16,688, 1995.

Dunkerton, T. J. and D. D. Delisi, Climatology of the equatorial lower stratosphere, *J. Atmos. Sci.*, *42*, 376-406, 1985.

Fritts, D. C., L. Yuan, M. H. Hitchman, L. Coy, E. Kudeki, and R. F. Woodman, Dynamics of the equatorial mesosphere observed using the Jicamarca MST radar during June and August 1987, *J. Atmos. Sci.*, *49*, 2353-2371, 1992.

Fritts, D. C., et al., Equatorial dynamics observed by rocket, radar, and satellite during the CADRE/MALTED campaign, 2, Mean and wave structures, coherence, and variability, *J. Geophys. Res.*, this issue.

Gill, A. E., *Atmosphere-Ocean Dynamics*, 662 pp., Academic, San Diego, Calif., 1982.

Garcia, R. R., and R. T. Clancy, Seasonal variation in equatorial mesospheric temperatures observed by SME, *J. Atmos Sci.*, *47*, 1666-1673, 1990.

Groves, G. V., Annual and semiannual zonal wind components and corresponding temperature and density variations, 60-130 km, *Planet. Space Sci.*, *20*, 2099-2112, 1972.

Hadley, G., Concerning the cause of the general trade-winds, *Philos. Trans. R. Soc.*, *29*, 58-62, 1735.

Hamilton, K., Rocketsonde observations of the mesospheric semiannual oscillation at Kwajalein, *Atmos. Ocean*, *20*, 281-286, 1982.

Harvey, V. L., and M. H. Hitchman, A climatology of the Aleutian High, *J. Atmos. Sci.*, *53*, 2088-2101, 1996.

Haurwitz, B., Frictional effects and the meridional circulation in the mesosphere, *J. Geophys. Res.*, *66*, 2381-2391, 1961.

Hays, P. B., V. J. Abreu, M. E. Dobbs, D. A. Gell, H. J. Grassl, and W. R. Skinner, The High Resolution Doppler Imager on the Upper Atmosphere Research Satellite, *J. Geophys. Res.*, *98*, 10,713-10,723, 1993.

Hays, P. B., D. L. Wu, and the HRDI Science Team, Observations of the diurnal tide from space, *J. Atmos. Sci.*, *51*, 3077-3093, 1994.

Helmholtz, H. v., Uber atmospharische Bewegungen, II, pp. 761-780, Sitz.-Ber. Akad. Wiss. Berlin, 761-780, 1888. (Translationed by C. Abbe, The mechanics of the Earth's atmosphere, pp. 94-111, Smithson. Inst., Washington, D.C., 1893.)

Hirota, I., Equatorial waves in the upper stratosphere and mesosphere in relation to the semiannual oscillation of the zonal wind, *J. Atmos. Sci.*, *35*, 714-722, 1978.

Hitchman, M. H., and C. B. Leovy, Evolution of the zonal mean state in the equatorial middle atmosphere during October 1978 - May 1979, *J. Atmos. Sci.*, *43*, 3159-3176, 1986.

Hitchman, M. H., and C. B. Leovy, Estimation of the Kelvin wave contribution to the semiannual oscillation, *J. Atmos. Sci.*, *45*, 1462-1475, 1988.

Hitchman, M. H., J. C. Gille, C. D. Rodgers, and G. Brasseur, The separated polar winter stratopause: A gravity wave driven climatological feature, *J. Atmos. Sci.*, *46*, 410-422, 1989.

Hitchman, M. H., K. W. Bywaters, D. C. Fritts, L. Coy, E. Kudeki, and F. Sürücü, Mean winds and momentum fluxes over Jicamarca, Peru, during June and August 1987, *J. Atmos. Sci.*, *49*, 2372-2383, 1992.

Hitchman, M. H., M. McKay, and C. R. Trepte, A climatology of stratospheric aerosol, *J. Geophys. Res.*, *99*, 20,689-20,700, 1994.

Hollingsworth, A., D. B. Shaw, P. Lonnberg, L. Illam, K. Arpe, and A. J. Simmons, Monitoring of observations and analysis quality by a data assimilation system. *Mon. Weather Rev.*, *114*, 861-879, 1986.

Holton, J. R., The influence of gravity wave breaking on the general circulation of the middle atmosphere, *J. Atmos. Sci.*, *40*, 2497-2507, 1983.

Hoppe, U. P., and D. C. Fritts, High resolution measurements of vertical velocity with the European incoherent scatter VHF radar, 1, Motion field characteristics and measurement biases. *J. Geophys. Res.*, *100*, 16,813-16,825, 1995.

Iwasaki, T., S. Yamada, and K. Tada, A parameterization scheme of orographic gravity wave drag with two different vertical partitionings, II, Zonally averaged budget analyses based on transformed Eulerian mean method, *J. Meteorol. Soc. Jpn.*, *67*, 29-40, 1989.

Kitaoka, T., Some considerations on the stratospheric circulation, related to the cause of the Aleutian High, *Meteorol. Abh.*, *36*, 121-152, 1963.

Kudeki, E., F. Sürücü, and R. F. Woodman, Mesospheric wind and aspect sensitivity measurements at Jicamarca using radar interferometry and poststatistics steering techniques, *Radio Sci.*, *25*, 595-612, 1990.

Kudeki, E., P. K. Rastogi, and F. Sürücü, Systematic errors in radar wind estimation: Implications for comparative measurements, *Radio Sci.*, *28*, 169-179, 1993.

Leovy, C. B., Simple models of thermally driven mesospheric circulation, *J. Atmos. Sci.*, *21*, 327-341, 1964.

Lieberman, R. S., and P. B. Hayes, An estimate of the momentum deposition in the lower thermosphere by the observed diurnal tide, *J. Atmos. Sci.*, *51*, 3094-3105, 1994.

Lieberman, R. S., M. D. Burrage, D. A. Gell, P. B. Hays, A. R. Marshall, D. A. Ortland, W. R. Skinner, D. L. Wu, R. A. Vincent, and S. J. Franke, Zonal mean winds in the equatorial mesosphere and lower thermosphere observed by the High Resolution Doppler Imager, *Geophys. Res. Lett.*, *20*, 2849-2852, 1993.

Lindzen, R. S., and J. R. Holton, A theory of the quasi-biennial oscillation, *J. Atmos. Sci.*, *25*, 1095-1107, 1968.

Maekawa, Y., S. Fukao, M. Yamamoto, M. D. Yamanaka, T. Tsuda, S. Kato, and R. F. Woodman, First observation of the upper stratospheric vertical wind velocities using the Jicamarca VHF radar, *Geophys. Res. Lett.*, *20*, 2235-2238, 1993.

Naujokat, B., An update of the observed quasi-biennial oscillation of the stratospheric winds over the tropics, *J. Atmos. Sci.*, *43*, 1873-1877, 1986.

Newell, R. E., and S. Gould-Stewart, A stratospheric fountain?, *J. Atmos. Sci.*, *38*, 2789-2796, 1981.

Newell, R. E., J. W. Kidson, D. G. Vincent, and G. J. Boer, *The General Circulation of the Tropical Atmosphere and Interactions With Extratropical Latitudes*, vol.1, 258 pp., MIT Press, Cambridge, Mass., 1972.

Ogino, S., M. D. Yamanaka, and S. Fukao, Meridional variation of lower stratospheric gravity wave activity: A quick look at Hakuho-Maru J-COARE cruise rawinsonde data, *J. Meteorol. Soc. Jpn.*, *73*, 407-413, 1995.

Ortland, D. A., W. R. Skinner, P. B. Hays, M. D. Burrage, R. S. Lieberman, A. R. Marshall, and D. A. Gell, Measurements of stratospheric winds by the high resolution Doppler imager, *J. Geophys. Res.*, *101*, 10,351-10,364, 1996.

O'Sullivan, D., and T. Dunkerton, Generation of inertia-gravity waves in a simulated life cycle of baroclinic instability, *J. Atmos. Sci.*, *52*, 3695-3716, 1995.

Palmer, T. N., G. J. Shutts, and R. Swinbank, Alleviation of a systematic westerly bias in general circulation and numerical weather prediction models through an orographic gravity wave drag parameterization, *Q. J. R. Meteorol. Soc.*, *87*, 125-135, 1986.

Politowicz, P. A., and M. H. Hitchman, Exploring the effects of forcing quasibiennial oscillations in a two-dimensional model, *J. Geophys. Res.*, *102*, 16,481-16,497, 1997.

Postel, G. A., Zonally asymmetric large-scale dynamics in the upper troposphere and lower stratosphere, M.S. thesis, 77 pp., Univ. of Wis.-Madison, 1994.

Riggin, D., D. C. Fritts, C. D. Fawcett, E. Kudeki, and M. H. Hitchman, Radar observations of gravity waves over Jicamarca, Peru, during the CADRE campaign, *J. Geophys. Res.*, this issue.

Spano, E., M. Crochet, and O. Ghebrebrhan, Some characteristics of the matrix used for the full decoding of truncated ranges, in *Solar-Terrestrial Energy Program: Proc. Fifth Workshop of Technical and Scientific Aspects of MST Radar*, p. 439, SCOSTEP Secretariat, NOAA/NGDC, Boulder, Colo., 1991.

Tanaka, H., and M. D. Yamanaka, Atmospheric circulation in the lower stratosphere induced by the mesoscale mountain wave breakdown, *J. Meteorol. Soc. Jpn.*, *63*, 1047, 1985.

Teweles, S., Anomalous warming of the stratosphere over North America in early 1957, *Mon. Weather Rev.*, *86*, 377-396, 1958.

Trenberth, K. E., and J. G. Olson, An evaluation and intercomparison of global analyses from the National Meteorological Center and the European Centre for Medium-Range Weather Forecasts, *Bull. Am. Meteorol. Soc.*, *69*, 1047-1057, 1988.

Trepte, C. R., and M. H. Hitchman, Tropical stratospheric circulation deduced from satellite aerosol data, *Nature*, *335*, 626-628, 1992.

Trepte, C. R., R. E. Veiga, and M. P. McCormick, The poleward dispersal of Mount Pinatubo Volcanic Aerosol, *J. Geophys. Res.*, *98*, 18,563-18,573, 1993.

Vincent, R. A., and D. Lesicar, Dynamics of the equatorial mesosphere: First results with a new generation partial reflection radar, *Geophys. Res. Lett.*, *18*, 825-828, 1991.

Vincent, R. A., and I. M. Reid, HF Doppler measurements of mesospheric gravity wave momentum fluxes, *J. Atmos. Sci.*, *40*, 1321-1333, 1983.

Woodman, R. F., and A. Guillen, Radar observations of winds and turbulence in the stratosphere and mesosphere, *J. Atmos. Sci.*, *31*, 493-505, 1974.

Yao, C.-Y., Geographical variation in the annual and quasi-biennial cycles in the tropical lower stratosphere, M.S. thesis, 130 pp., Univ. of Wis.-Madison, 1994.

L. Harvey, M. Hitchman (corresponding author), J. Kugi, G. Postel, C. Yao, Department of Atmospheric and Oceanic Sciences, University of Wisconsin - Madison, 1225 W. Dayton Street, Madison, WI 53706. (e-mail: harvey@eos4.larc.nasa.gov; matt@adams.meteor.wisc.edu; greg@redoubt.meteor.wisc.edu; chiayi@ms2.hinet.net)

C. Fawcett and E. Kudeki, Department of Electrical and Computer Engineering, University of Illinois, 1406 W. Green Street, Urbana, IL 61801. (e-mail: erhan@deln.ece.uiuc.edu; fawcett@deln.ece.uiuc.edu)

D. Fritts and D. Riggin, Colorado Research Associates, 3880 Mitchell Lane, Boulder, CO 80301. (email: dave@michelangelo.colorado.edu; dennis@leonardo.colorado.edu)

D. Ortland, Space Physics Research Laboratory, Department of Atmospheric, Oceanic and Space Sciences, University of Michigan, 2455 Hayward Street, Ann Arbor, MI 48109-2143. (email: ortland@sprlj.sprl.umich.edu)

(Received May 21, 1996; revised June 18, 1997; accepted June 18, 1997.)